Report on the initial hydrogeological and agricultural conditions of the Italian site

Deliverable D_3.1.3

Contributing partners:

PP1 – CNR IGG

LP – UNIPD DICEA

TABLE OF CONTENTS

1. Foreword

The present report consists of updating the CNR contribution to "Intermediate report on the initial hydrogeological and agricultural conditions of the Italian site (D_3.1.3)". The updated information has been inserted in the proper sections of the previous version, which was delivered on 02.2020.

2. Introduction

The Interreg Italy-Croatia project MoST (Monitoring Sea-water intrusion in coastal aquifers and Testing pilot projects for its mitigation) aims at testing solutions against saltwater intrusion in agricultural areas, a worldwide problem exacerbated by human activities and climate changes. The regions of interest of MoST project are the Veneto Region coastal plain south of the Lagoon of Venice (Italy) and the Neretva river mouth (Croatia).

MoST WP3.1 Action (Site characterization) aims at characterizing both the regions of interest on the basis of the available knowledge and previous studies. This report regards the characterization of the hydrogeological setting of the Italian study area, which is part of the Deliverable D_3.1.3 "Report on the initial hydrogeological and agricultural conditions of the Italian site" planned to be issued by the WP3 "Studying".

The aim of this report is to sketch the hydrogeological setting in order to provide the basis for the in-situ activities and numerical modelling. The characterization of the hydrogeological setting of the Italian study area was first outlined on a regional scale and secondly detailed for the pilot area. Specifically, the report includes a short description of the study area, a regional sketch of the setting of the Venice aquifer system and the saltwater contamination, a detailed hydrostratigraphic model of the phreatic and semiconfined aquifers of the pilot test areas.

3. Materials and methods

The hydrogeological characterization of the study area has been obtained through the interpretation of multidisciplinary data available from previous investigations and new in-situ measurements.

Electrical Conductivity (EC) represents a practical and reliable measure for the estimate of water salinity, therefore, within this project, it has been selected to mark the limit between freshwater and

saltwater values in relation to tolerance bounds for crop growth. Specifically, the classification adopted by Carbognin and Tosi (2003) has been used in order to allow a comparison between past and new measurements. They identified three classes of water quality:

1) salty if EC exceeds 5 mS/cm;

2) brackish if EC ranges between 2 and 5mS/cm with salt concentration higher than 1 g/L;

3) fresh when EC is less than 2 mS/cm and the water is suitable for irrigation purposes.

Regarding the classification of the electrical resistivity measured by geophysical methods (vertical electrical sounding, electrical tomography, airborne electromagnetic, etc.) we assumed electrical resistivity <5 Ω·m and >10 Ω·m, as the upper value for saltwater and the lower value for freshwater, respectively (as already done by Carbognin and Tosi, 2003; de Franco et al., 2009; Teatini et al., 2011).

Data obtained by previous investigations refer to the following.

- Projects: ISES, BRENTA, CARG, Corila Research Lines 3.1 and 3.10, GeoRisk.
- Databases: http://webgis.cittametropolitana.ve.it/geologia, http://difesasuolo.provincia.venezia.it/DifesaSuolo/Index?pagina=1&id=banca_dati_idrogeologica (Città Metropolitana Venezia); http://www.isprambiente.gov.it/Media/carg/veneto.html (Istituto Superiore per la Protezione e la Ricerca Ambientale); http://cigno.atlantedellalaguna.it (CNR); http://gisgeologia.regione.veneto.it/website/venezia-10k/viewer.htm (Regione del Veneto).
- Publications: Carbognin and Tosi, 2003; Rizzetto et al., 2003; Carbognin et al., 2006; Carbognin et al., 2010; Mayer et al., 2006; Tosi et al., 2007; de Franco et al., 2009; Tosi et al., 2009; Teatini et al., 2010; Viezzoli et al., 2010; Teatini et al., 2011; Tosi et al., 2011; Da Lio et al., 2013; Da Lio et al., 2015; Tosi et al., 2018.

The new data, which will represent the reference baselines of the saltwater conditions characterizing the pilot area before the implementation of the salinity mitigations measures, have been acquired during the MoST monitoring activities started in July 2019.

4. Study area

The study area encompasses the territory between the southern Venice lagoon margin and the terminal part of the Adige River. Specifically, the pilot test area is located just south of the Brenta and Bacchiglione rivers in a low-lying farmland (Fig. 1).

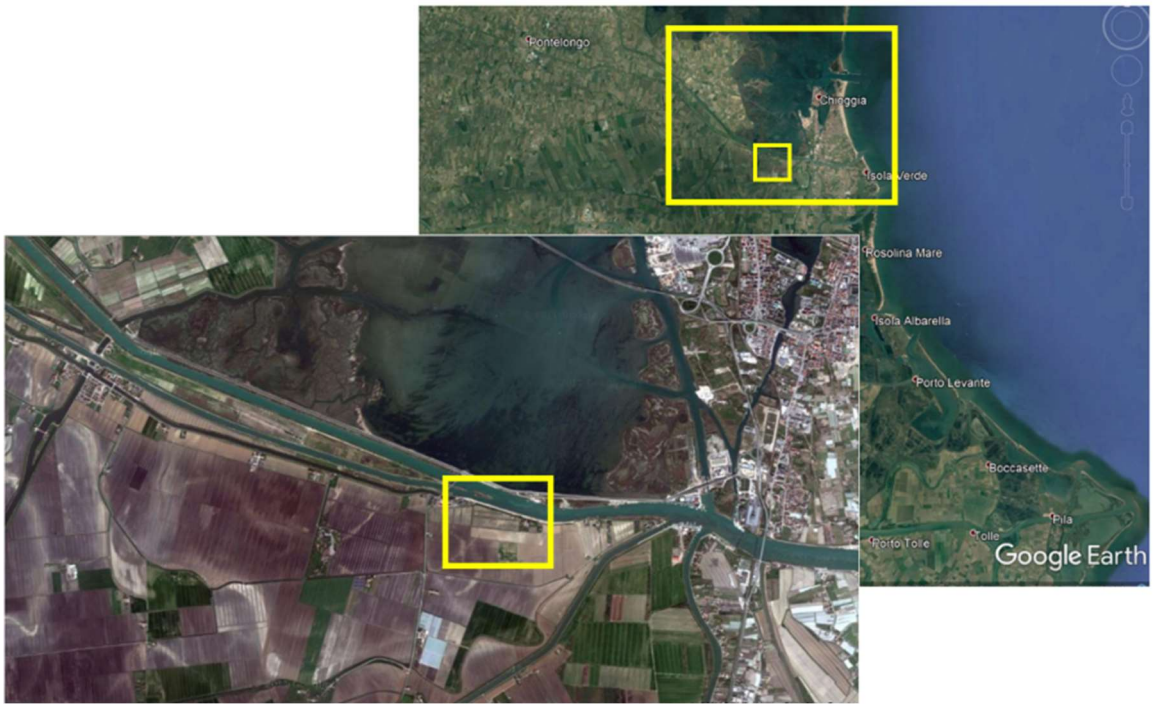

Fig. 1 - Location of the study and the pilot test area.

Over the historical time, river diversions, channeling, and land reclamation progressively changed the hydrogeological setting of the study area, and presently most of this coastal plain sector lays up to 3 m below the mean sea level (e.g., Gasparetto-Stori et al., 2012). Therefore, a complex network of ditches and pumping stations, that discharge the drainage water into the Venice Lagoon or the Adriatic Sea, regulates the depth of the water table.

The artificially controlled groundwater and surface water flows combined with sea level rise and land subsidence have enhanced the saltwater intrusion and the related soil salinization with serious environmental and socio-economic consequences (Carbognin et al., 2006). In particular, saltwater intrusion threatens drinking water quality, enhances the risk of soil desertification, compromises the agricultural practices and decreases freshwater storage capacity (Carbognin and Tosi, 2003).

Understanding saltwater intrusion in the aquifer system and agricultural soil in this peculiar transitional coastal environment is challenging, since it is characterized by (1) very high heterogeneity of the subsoil and (2) anthropogenically controlled surface water - groundwater interaction.

5. Regional hydrogeological setting of the aquifer system

A reconstruction of the hydrogeological setting at the regional scale has been made on the basis of hundreds of available stratigraphic sections obtained from many artesian wells drilled down to -350 m deep, scattered over the area.

Most of the data regarding the deep aquifers have been retrieved by artesian wells drilled for groundwater pumping after the World War II and particularly during the industrial boom, and, anyway, before the groundwater regulation adopted in Venice in the 1970s (Da Lio et al., 2013 and references therein).

The Venice aquifer system includes six main sub-horizontal aquifers, most of them characterized by high productivity at regional scale, confined by silty-clayey material (Fig. 2).

- The 30-50 m thick upper hydro-stratigraphic unit is characterized by phreatic and locally confined aquifers. It shows a complex architecture, which is the result of the relationships among Late Pleistocene alluvial and Holocene lagoon, deltaic, and littoral depositional sequences. This unit shows a very high heterogeneity and is generally contaminated by saltwater.
- The first confined aquifer (Aquifer A) lies from 55 to 75 m below msl, it is characterized by low permeability and saltwater contamination.
- Aquifer 1, located from 80 to 125 m below msl, is spatially continuous and characterized by a considerable productivity. This is one of the most exploited aquifers in the past.
- Aquifer 2 includes a complex of minor sandy layers located between 130 and 155 m below msl that were organized in different groups by the likely arrival of the sediments to a single depositional cycle.
- Aquifer 3 spans the depth range from 165 to 180 m below msl and generally reduces its permeability seaward.
- Aquifer 4, located between 205 and 235 m below msl, is the most productive aquifer in the Venice area.

- Aquifer 5 is characterized by an irregular lithology and is located between 255 and 305 m below msl.
- Aquifer 6, placed between 315 and 340 m below msl, is tapped only in the mainland where the grain size of the deposits provides good productivity.

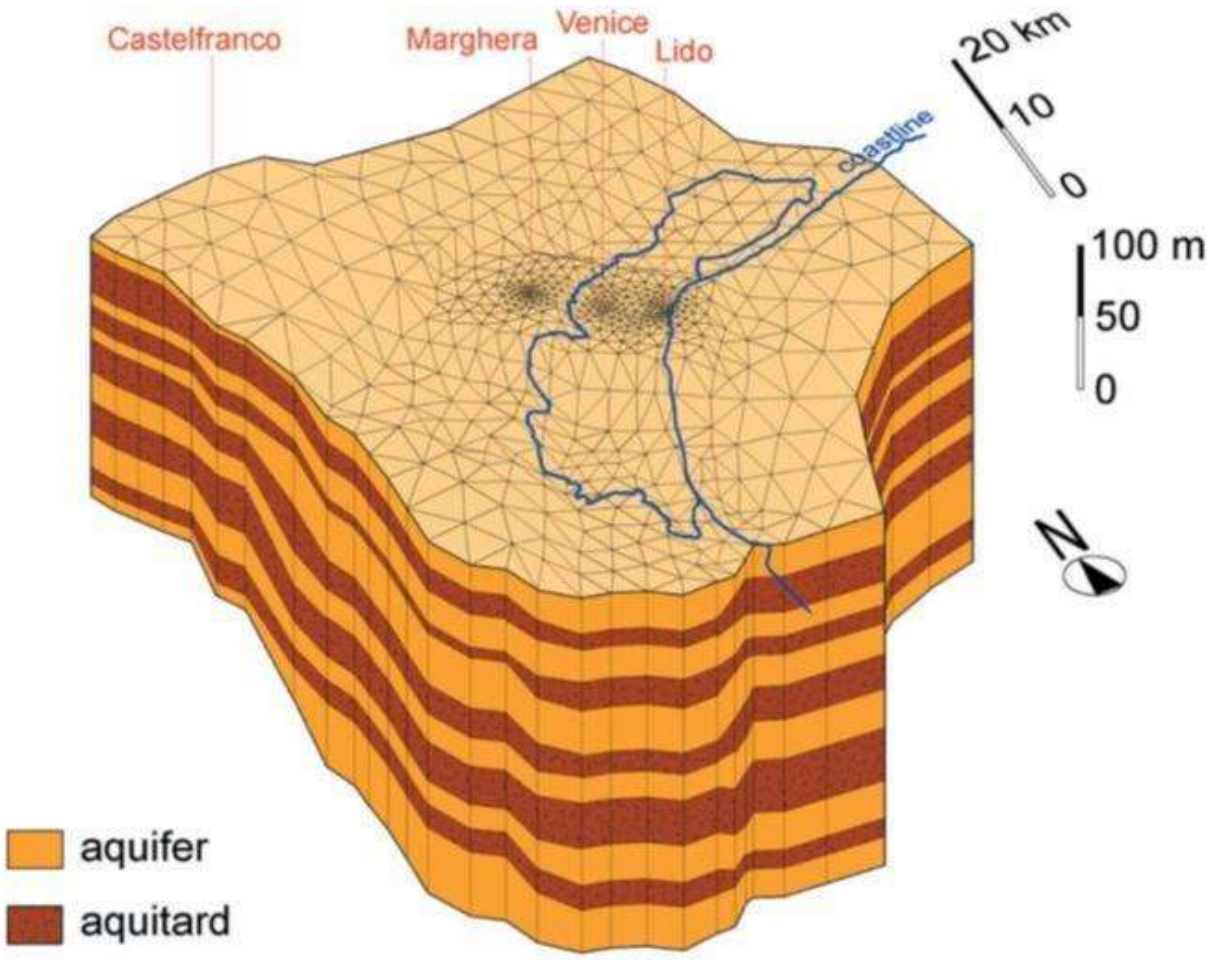

Fig. 2 - *Perspective three-dimensional view of the regional finite element model used to simulate the groundwater flow in the Venice multi-aquifer system (Teatini et al., 1995).*

Fig. 3 shows the hydro-stratigraphic setting of the aquifer system upper units crossing the study area. The phreatic aquifer and locally confined aquifers are characterized by a complex architecture due to the presence of lateral heteropies and vertical transitions (alluvial, lagoon, deltaic, and littoral deposits) consisting of alternating sandy-silty, clayey-silty and clayey layers (Tosi et al., 2007).

Therefore, the reconstruction of these aquifers at the regional scale would be unrealistic and it has been opted to do it only at the spatial scale of the pilot test area.

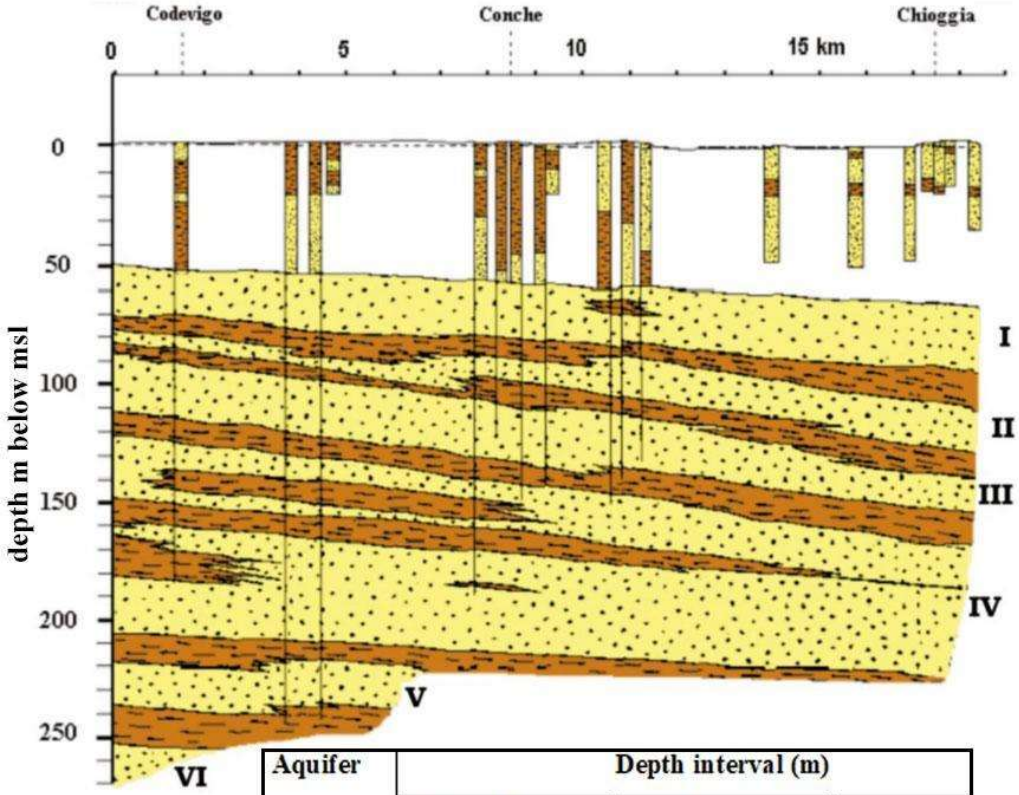

Aquifer	Depth interval (m)		
	Piove di Sacco	*Conche*	*Chioggia*
I	40 - 60	57 - 80	68 - 95
II	65 -100	90 - 135	113 - 155
III	107 - 140	143 - 164	170 - 190
IV	150 - 197	175 - 215	190 - 228
V	210 - 230	228 - 245	-
VI	243 - 263	-	-

Fig. 3 - *Setting of the aquifer system in the nearby of the study area.*

Several hundreds of vertical electrical soundings (VES) allowed to map the saline water presence in the Venice aquifer system. The saline water sketched in Fig. 4 shows that saline contamination is not limited to the first 50-100 m aquifer depths but also involves deeper aquifers from 400 m to more

than 1000 m because of the presence of paleo seawaters (Agip, 1994; Benvenuti et al., 1973; Bxio et al., 1999).

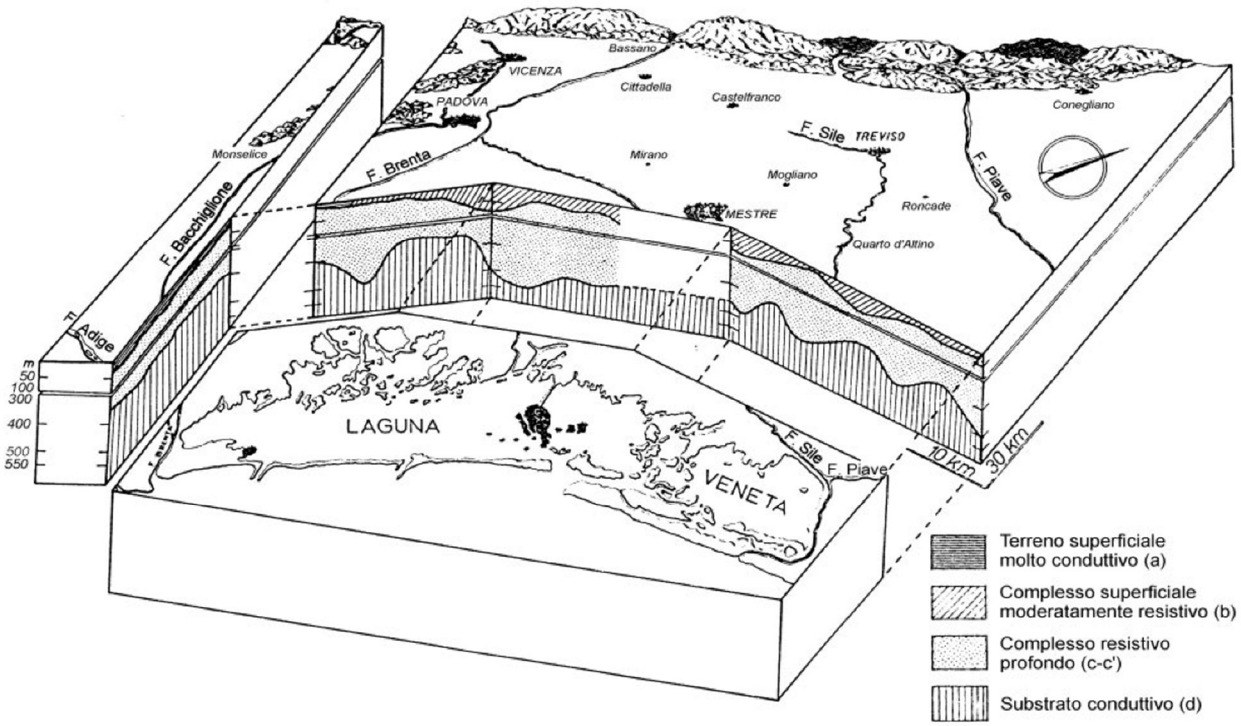

Fig. 4 - *Electro-stratigraphic model of saline contamination in the Venice aquifer system (Benvenuti et al., 1973).*

The integration of geophysical surveys with groundwater and surface water analysis allowed to map saline water extent. Fig. 5 and Fig. 6 clearly show that saltwater contamination plume affects the coastland up to 20 km inland from the sea-lagoon boundary.

The depth of the fresh/salt-water interface varied from 2 to 30 m below the ground level and exhibits a significant, mainly seasonal, time variation; the bottom of the contaminant plume penetrates from 10 even to 100 m depth in the subsoil (e.g., Carbognin and Tosi, 2003).

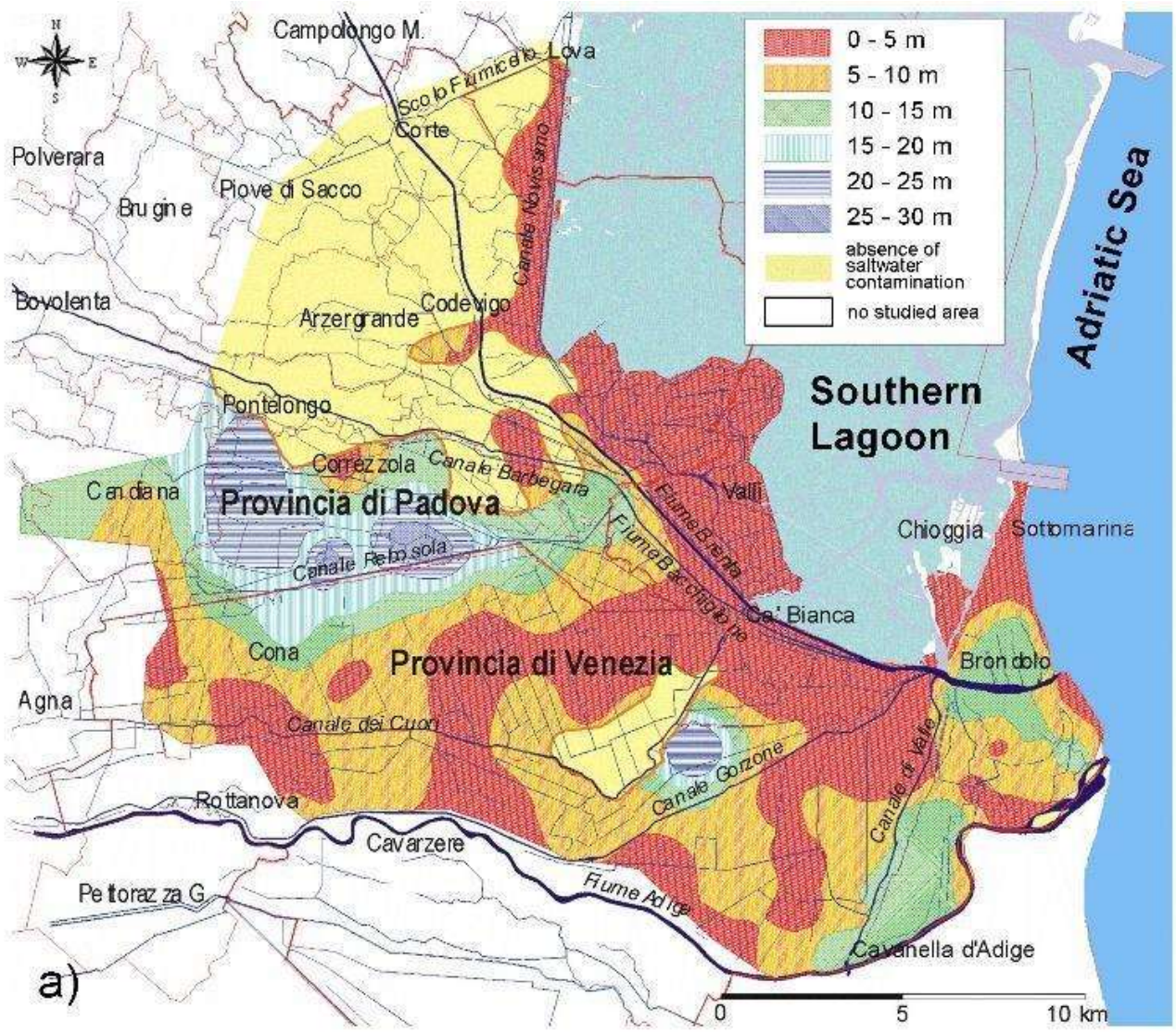

Fig. 5 - *Depth of the top of the electro conductive layer, which corresponds to freshwater - saltwater interface.*

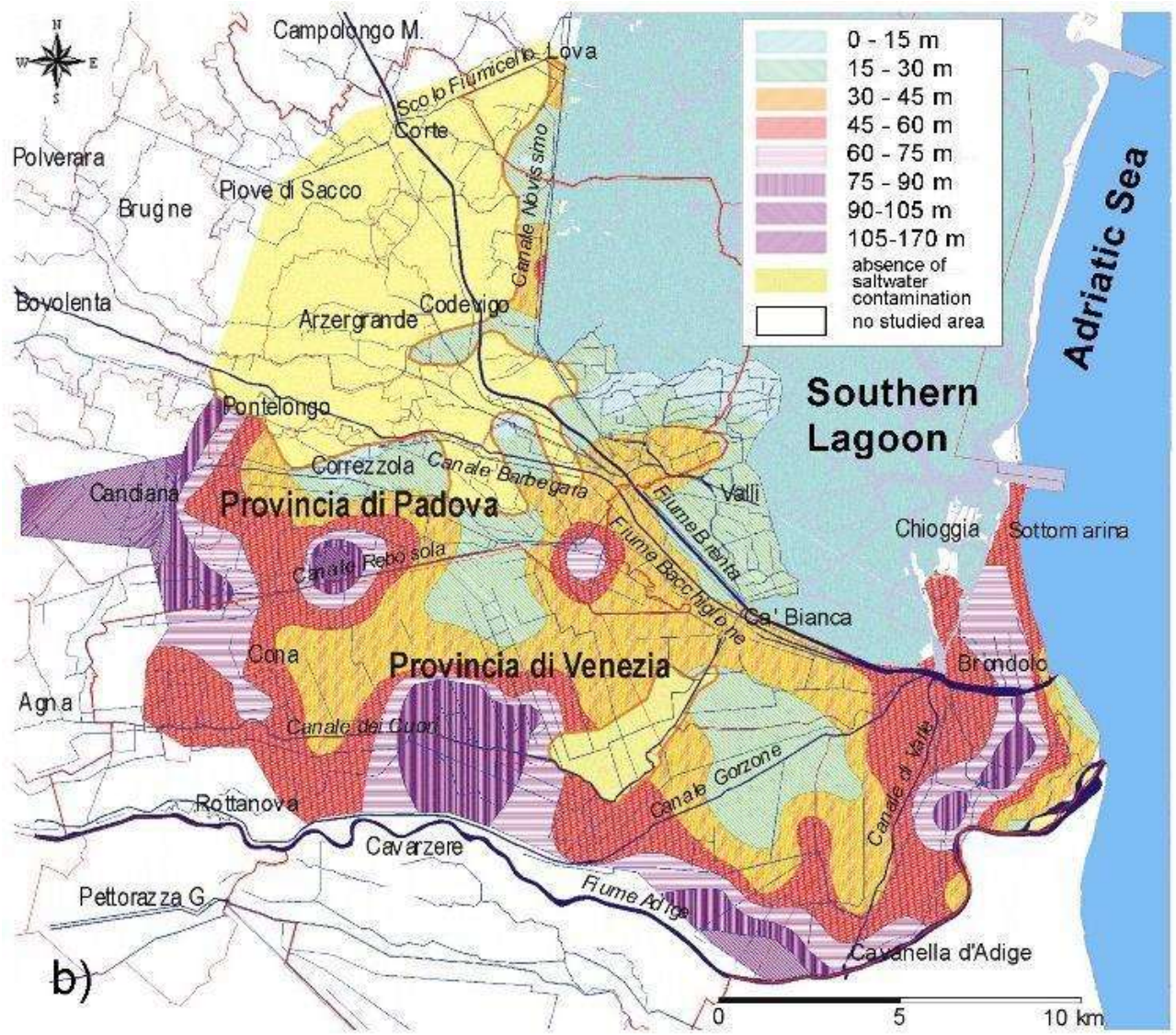

Fig. 6 - *Depth of the bottom of the electro conductive layer, which roughly corresponds to the maximum depth of the saltwater contamination.*

Although the availability of hundreds of VES together with hundreds of well and stratigraphic data allowed mapping the saltwater contamination at regional scale, a clear and comprehensive image of surficial water-groundwater interaction in a consistent and homogeneous framework, was far from being achieved. This is mainly because of i) in-situ surveys were acquired over different seasons and meteo-hydrographic conditions, and ii) the presence of hydro-morphological discontinuities such as the lagoon margin, rivers and channels limited the geophysical surveys. In order to overcome this issue, continental and marine surface water–groundwater interactions, an airborne electromagnetics

(AEM) survey was carried out by the SkyTEM system in 2013 over the Venice coastland (Tosi et al., 2018). Some results are shown in Fig. 7.

We assumed electrical resistivity <5 and > 10Ωm as the upper value for saltwater and the lower value for freshwater, respectively.

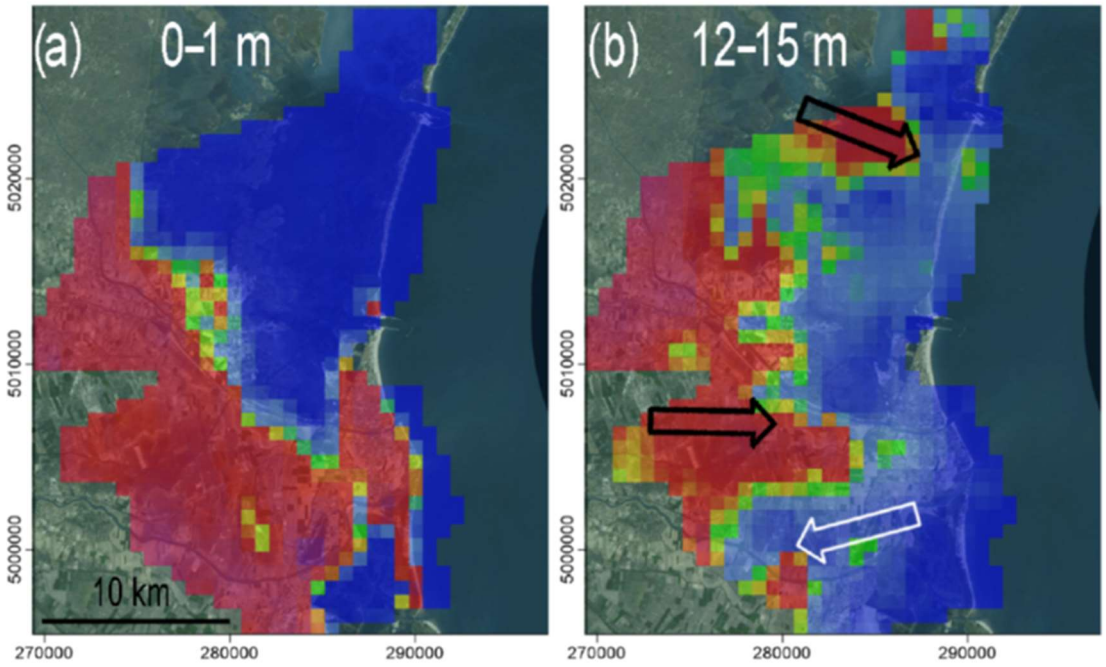

Fig. 7 - *Conceptualization of the freshwater-saltwater relationship at (a) 0–1 m, (b) 12–15 m, obtained by integrating the results of the AEM survey with in-situ information. Fresh-, brackish- and saltwaters are represented by red, green/yellow and blue colors, respectively. White and black arrows delineate the advancement of the saltwater intrusion and freshwater flow, respectively.*

The combined analysis of the saltwater mapping, geological setting, geomorphological structures and surface hydrology pointed out that the saltwater intrusion in the shallow aquifers is generally connected to:

(i) land elevation below the mean sea level,

(ii) seawater encroachment into the river mouths (Fig. 8),

(iii) presence of several sandy paleochannels (Fig. 9),

(iv) lowering of the water table by pumping stations.

The dynamics of the soil salinization process is especially sensitive to the changes in the river discharge, e.g., Brenta, Bacchiglione, Adige, Gorzone waterflows, water levels (as they are regulated

by the pumping stations) and climatic conditions (seasonal oscillations, and sea level rise) (Da Lio et al. 2015). An example of seawater encroachment along the Brenta and Bacchiglione rivers during a serious dry season is shown in Fig. 8.

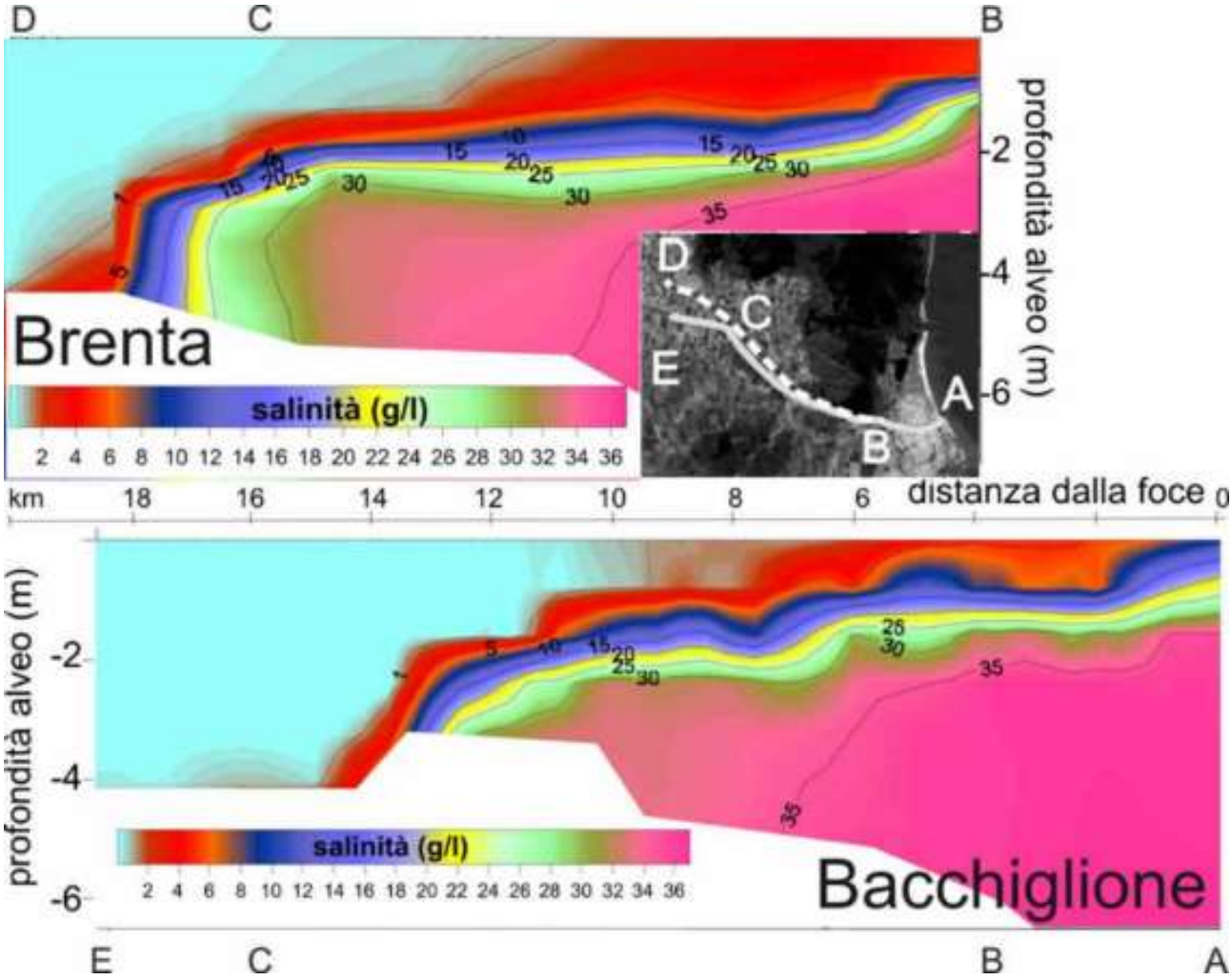

Fig. 8 - *Saltwater encroachment along the Brenta (a) and Bacchiglione (b) rivers in the dry and hot July 2003; in the satellite map, white dashed line and grey continuous lines show the survey paths.*

Multidisciplinary investigations highlighted that the shallow aquifers are generally contained in sandy geomorphological features, which are mostly paleo-channels and ancient coastal ridges, irregularly distributed in the paleo-coast because of their nature.

Most of these morphological structures extends from the mainland to the lagoon and shows a broad spatial development (e.g., Rizzetto et al., 2003; Tosi et al., 2009) (Fig. 9).

The presence of sandy buried paleochannel systems crossing the farmland, with a main direction from inland to the lagoon boundary, acts as preferential pathways for groundwater flow and solute transport, as detected in other similar coastal sites.

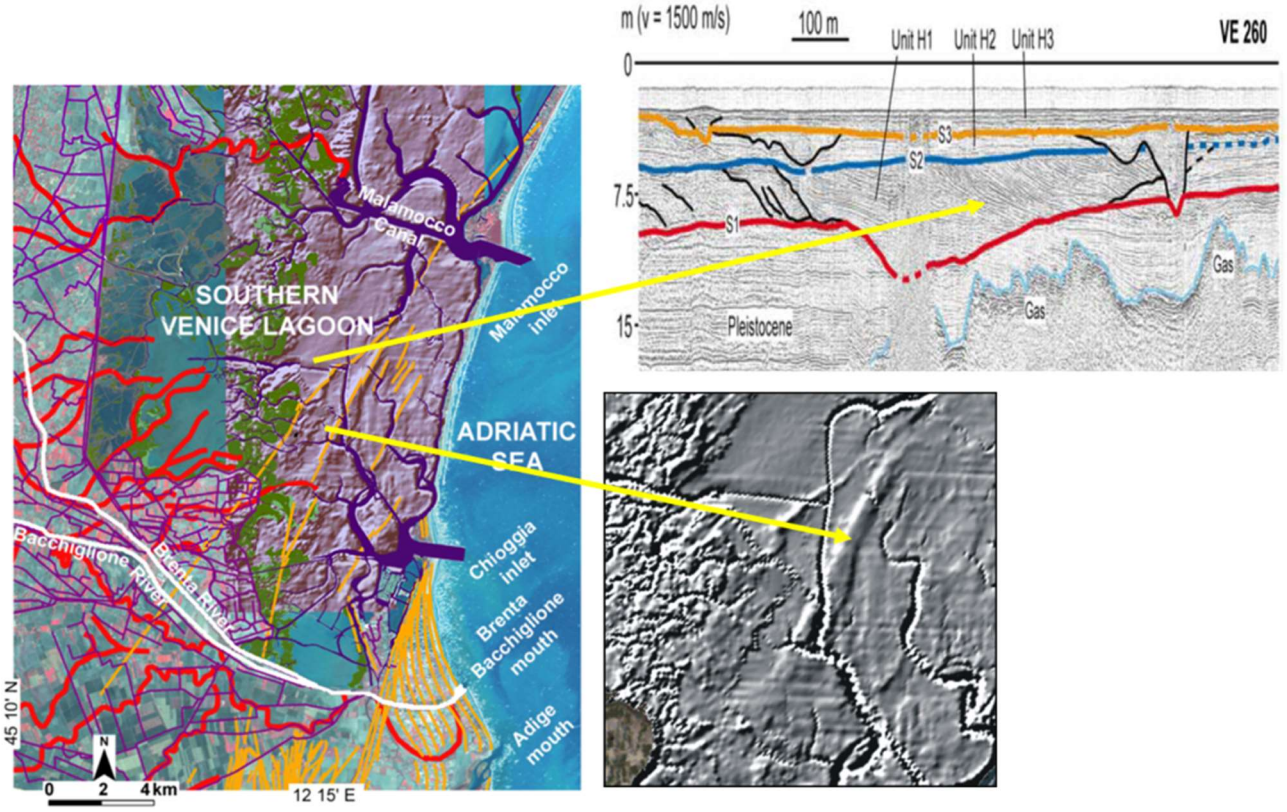

Fig. 9 - *ASTER satellite image of the southern Venice coastland. A shaded relief map of the lagoon bottom is superimposed on the image. Red lines: paleoriverbeds; orange lines: paleobeach ridges; dark violet and light violet areas: present lagoon channels and hydrographic network, respectively; green areas: salt marshes. White lines highlight the present courses of the Brenta and Bacchiglione rivers.*

6. Hydrogeological setting of the pilot test area

The aquifer system of the pilot test area framed in the regional hydro-stratigraphic setting is shown in Fig. 10. Focusing on the shallower units, which are the target of the project, alluvial, lagoon, deltaic, and littoral deposits, consisting of alternating sandy-silty, clayey-silty and clayey layers (Tosi et al., 2007), form the phreatic aquifer and locally confined aquifers.

At the pilot test site, the stratigraphy obtained down to 50 m depth outlines the following setting:

- phreatic aquifer (A1) in the shallower 12 m thick unit,
- semi-confined aquifer (A2) between 18 and 38 m depth,
- locally confined aquifer (A3) down to the bottom (Fig. 10).

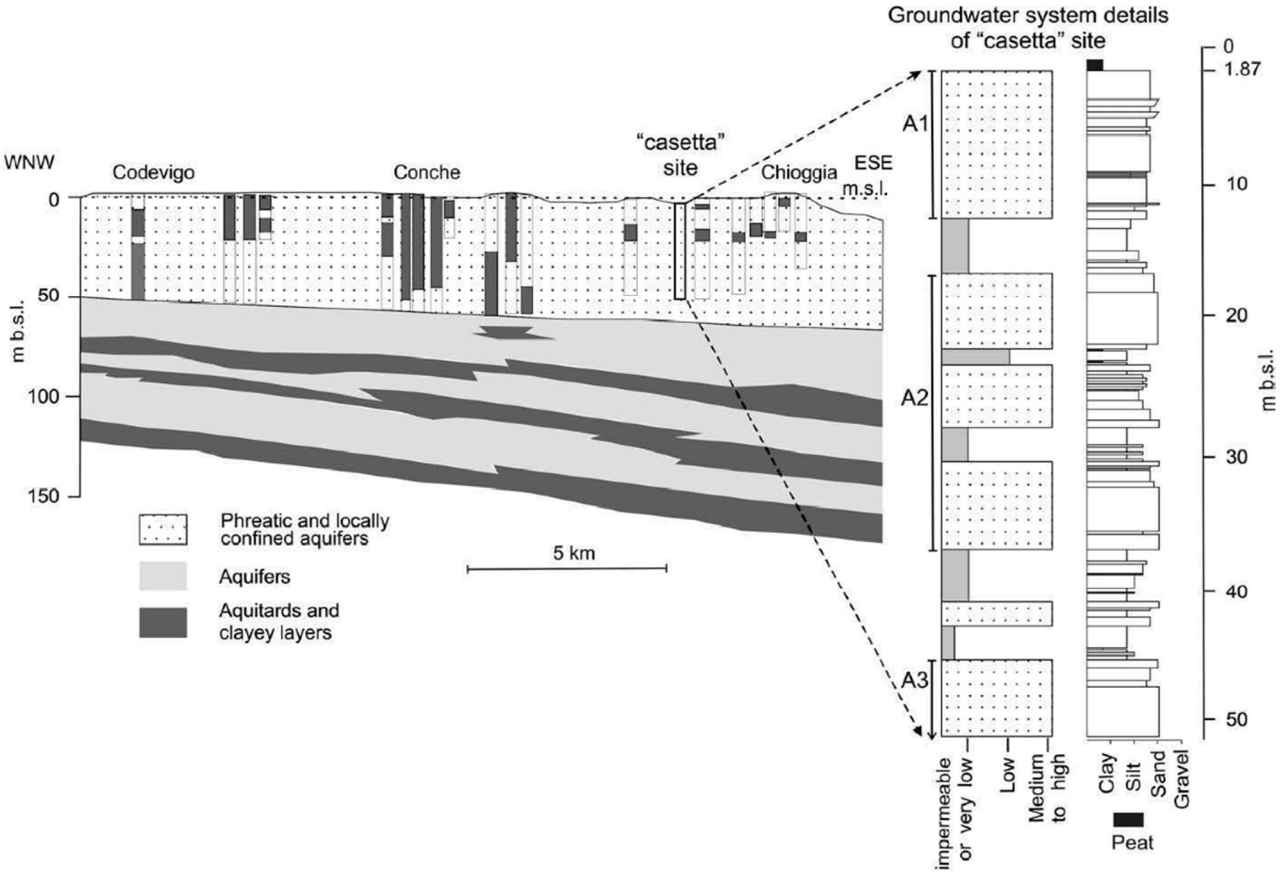

Fig. 10 - *East–west vertical section showing the hydrogeological setting of the upper 150 m depth along the southern margin of the Venice Lagoon. The blow up on the right shows the detailed lithostratigraphy and the hydrologic characterization of the Casetta site obtained by the borehole (CA50).*

Advances in understanding continental and marine water interaction has been provided by Airborne Electromagnetic (AEM) survey (Vezzoli et al., 2010). AEM allowed acquiring data over both water and land without discontinuity (spatial and temporal) and the transition between salt and fresh-saturated sediments below the lagoon and in the surrounding farmland is clearly depicted (Teatini et al., 2011). Exchanges between lagoon water and groundwater in the study area are shown in Fig. 11 and Fig. 12.

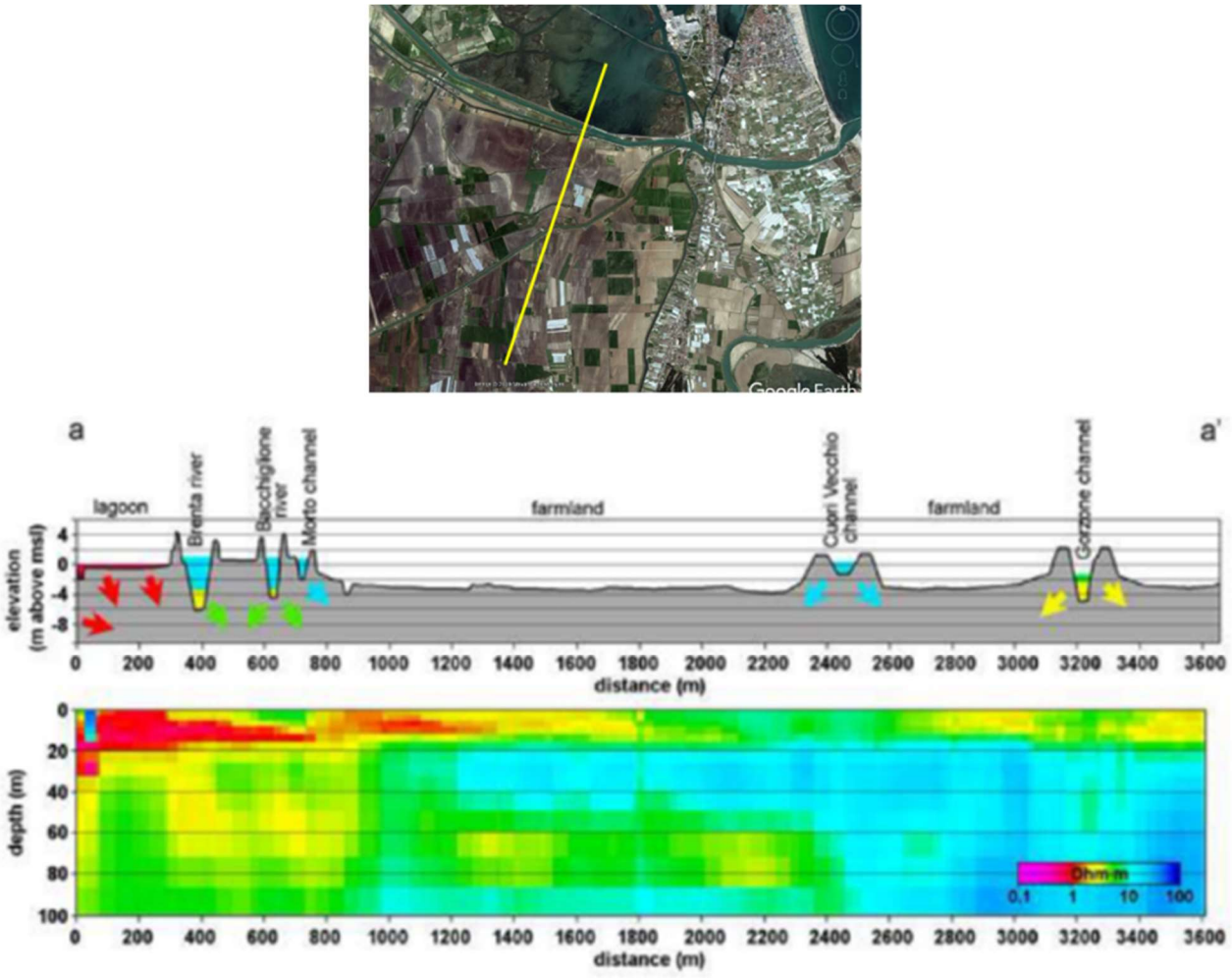

Fig. 11 - *Multi-layer vertical resistivity sections obtained from the AEM survey. The arrows show the flow direction.*

Regarding the very shallow aquifers, the presence of an overconsolidated clay between 20 and 10 m depth, i.e. the Caranto paleosoil (Donnici et al., 2011), exhibits an important hydrogeologic function and often precludes the downward propagation of seawaters. Hence, the salinity degree generally reduces below 20 m depth, at least in some portions of the study area, even if brackish waters are present also below 50 m depth.

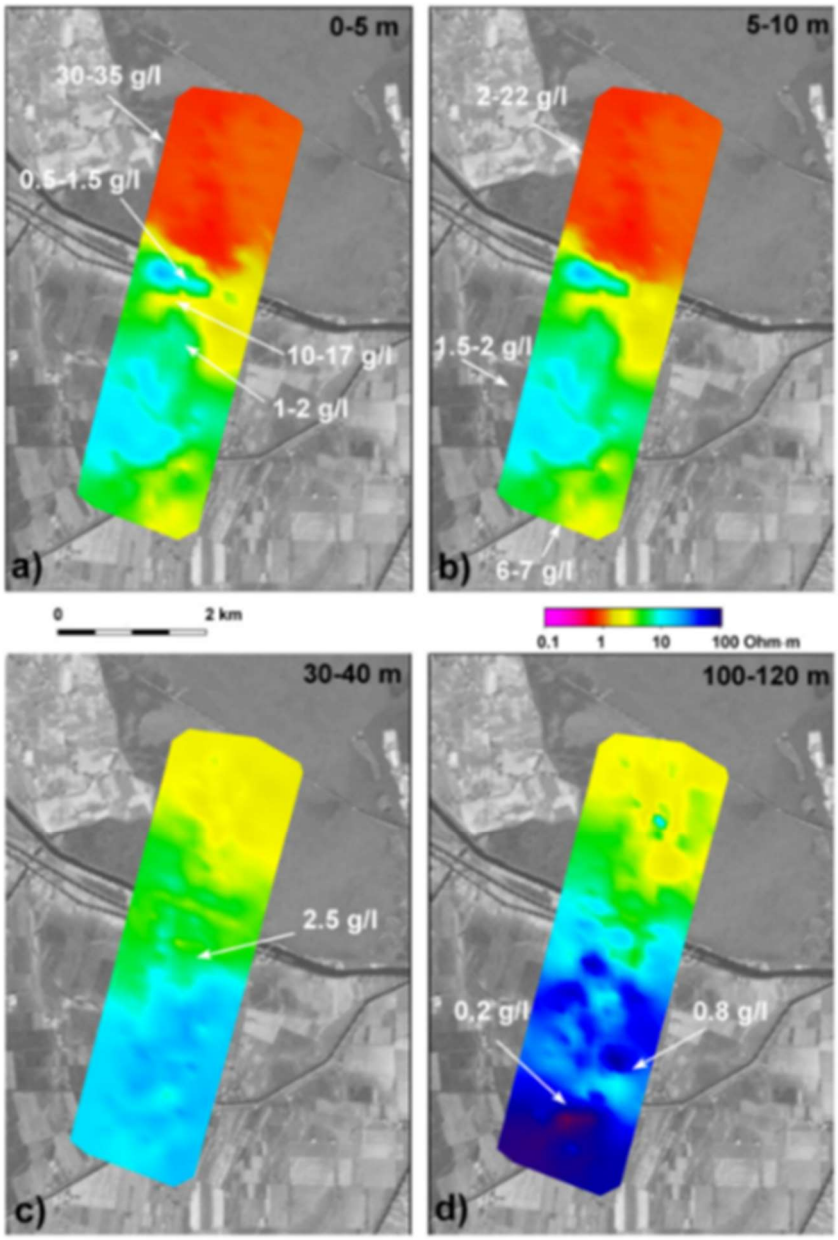

Fig. 12 - *Average resistivity maps for the 0–5 (a), 5–10 (b), 30–40 (c), and 100–120 (d) m depth intervals obtained by the SkyTEM system in the southern lagoon sector. The salinity values measured in some boreholes scattered in the study area are shown according to the well depth.*

AEM and in-situ data allowed for a detail hydrogeological sketch at the lagoon margin sector (Fig. 13). Groundwater moves preferentially from the lagoon sub-bottom towards the farmland because of (i) the higher density of the saltwater, (ii) the inland piezometric head lower than the surface water level due to a land elevation well below the mean sea level and (iii) a widespread use of pumping stations to keep low-lying lands drained. The range of permeability and salinity is shown in Fig. 14.

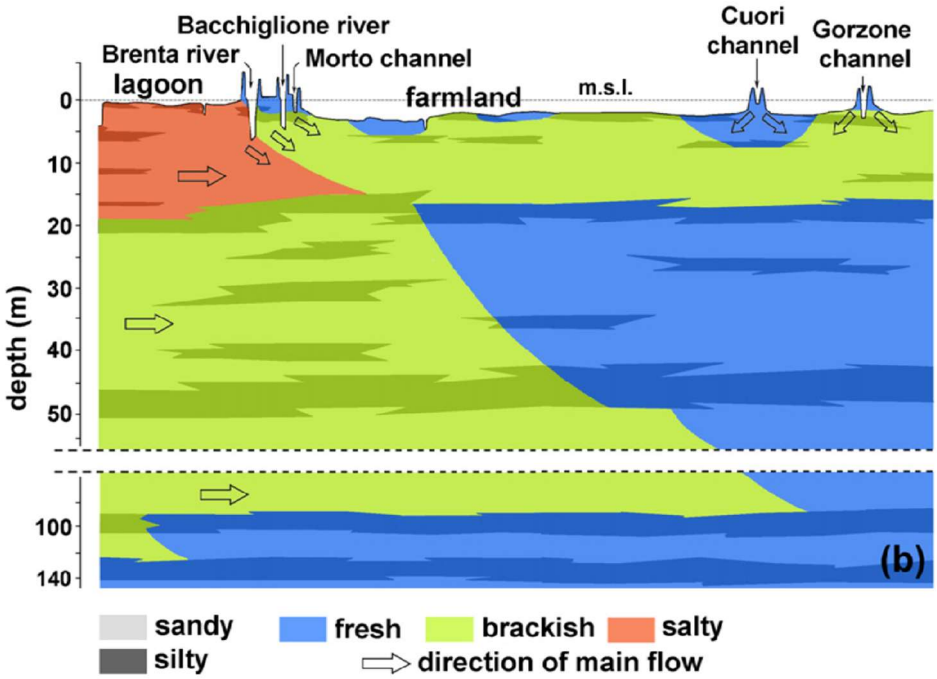

Fig. 13 - *Conceptualization of the hydrogeologic setting of the study area obtained by integrating the results of the AEM survey with sediment core data and groundwater analysis.*

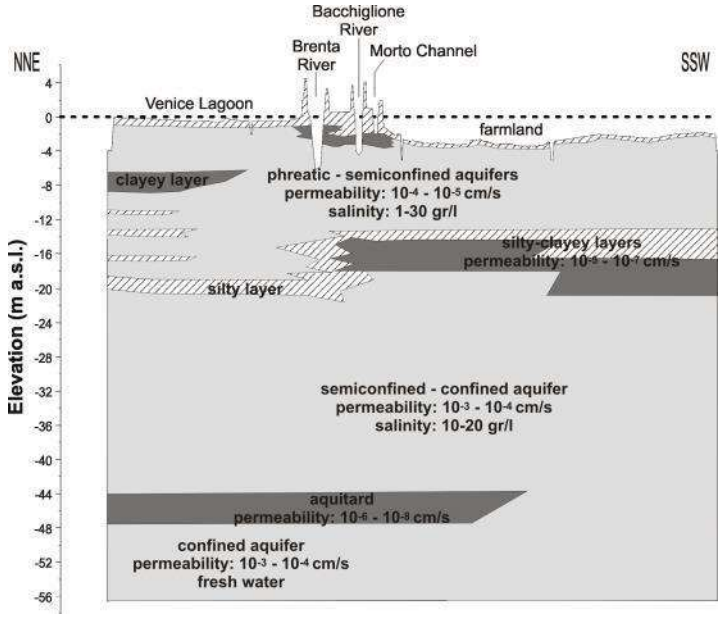

Fig. 14 - *Range of permeability and salinity of the subsoil layers at Casetta site.*

A detailed freshwater–saltwater relationship at the experimental site was depicted by time-lapse electrical resistivity tomography (TL-ERT).

The pilot test area is affected by seasonal resistivity fluctuation of the saltwater front that intrudes landward during the autumn–winter season and moves back seaward in spring–summer (de Franco et al., 2009) (Fig. 15).

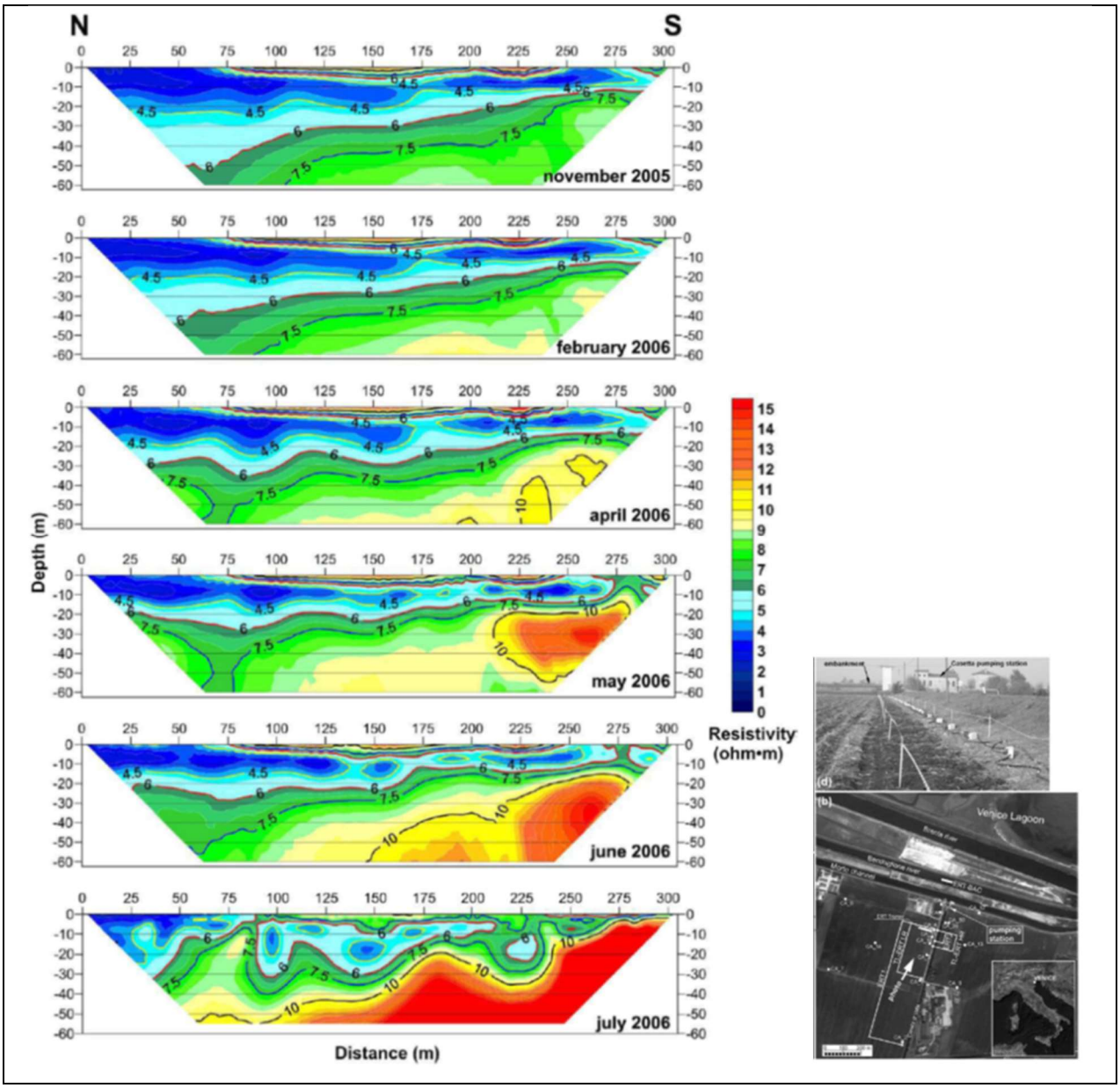

Fig. 15 - *Inverted resistivity models showing the evolution of seawater intrusion between November and July. N: North (lagoon margin); S: South (farmland).*

Detailed stratigraphic and EC logs, along with electrical resistivity tomography section, allowed a preliminary characterization of the saltwater variation of the pilot test area.

In particular, Fig. 16 shows EC logs reflecting the salinity degree in the three aquifers located at different depths, 0-8 m (A1), 15-20 m (A2), and 40-45 m (A3).

All these aquifers are salt-contaminated, despite in some of them brackish water occurs in the shallower part of the wells.

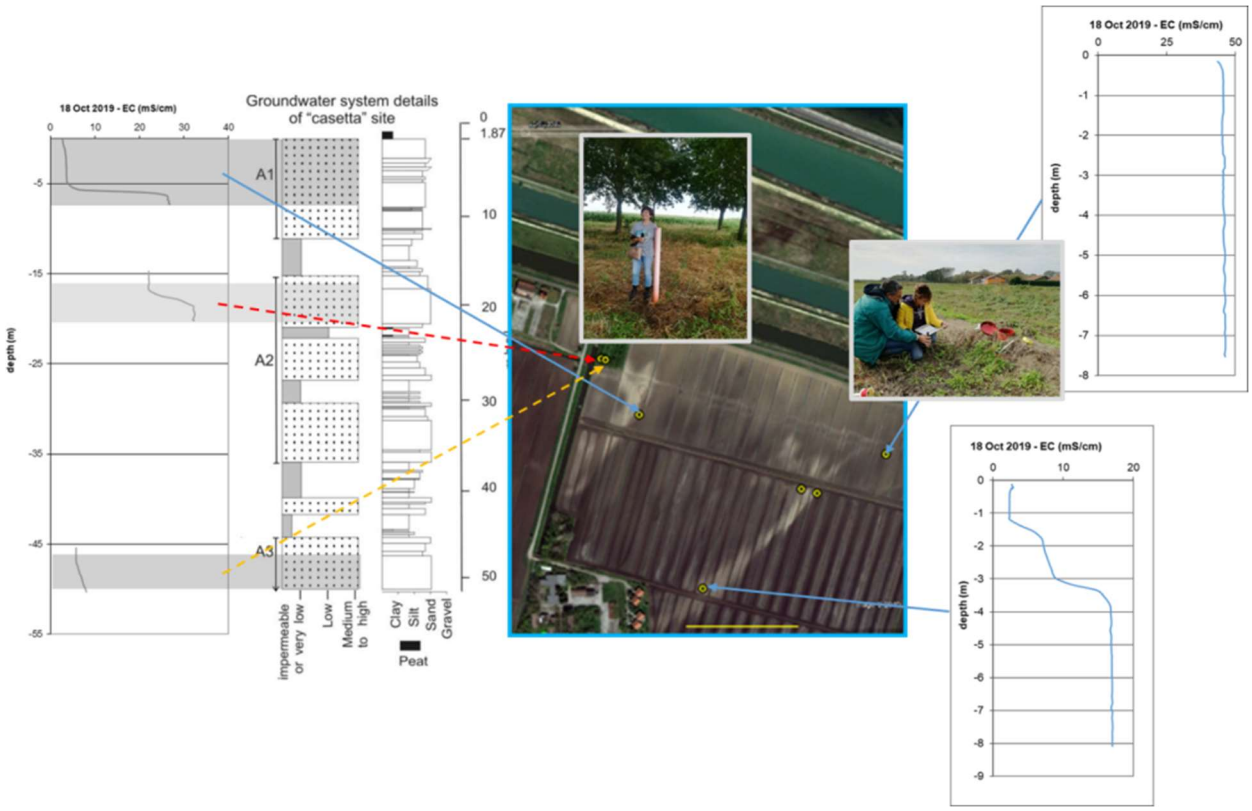

Fig. 16 - *Hydro-stratigraphic setting of the pilot test area.*

Water quality is significantly improved by local rainfalls that rapidly supply freshwater, which is then stored in the sandy paleo-ridge systems. Indeed, the latter ones are capable to contain groundwater with lower salinity than that occurring in the lateral silty deposits, at least in the shallow part.

Important recharge factors are the fresh-water releases for irrigation purpose and riverbed seepage. The latter is influenced by the tide dynamics, which, together with river discharge, control the seawater encroachment along the river mouths.

Relict geomorphological features, filled with high permeability sediments, provide a hydraulic connection between freshwater aquifers and sea, possibly facilitating saltwater intrusion landward or, conversely, acting as reservoir of freshwater from precipitation, irrigation, and percolation through river beds.

Thin lenses of fresh- to brackish- waters are present in the paleochannel bodies present in the pilot test area, with variable extent depending on their recharge (Fig. 17). Electrical resistivity tomography

crossing the paleochannel system in the pilot test area clearly shows the capability of these sandy bodies to store low salinity groundwater (Fig. 18).

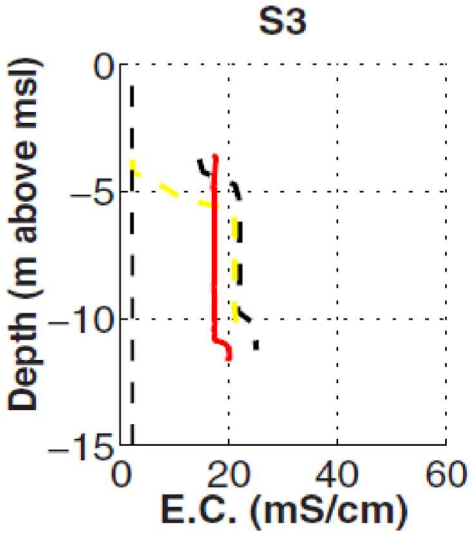

Fig. 17 - *Electrical conductivity logs showing the freshwater–saltwater dynamics in the paleochannel. The dashed line represents the maximum EC value for irrigation use.*

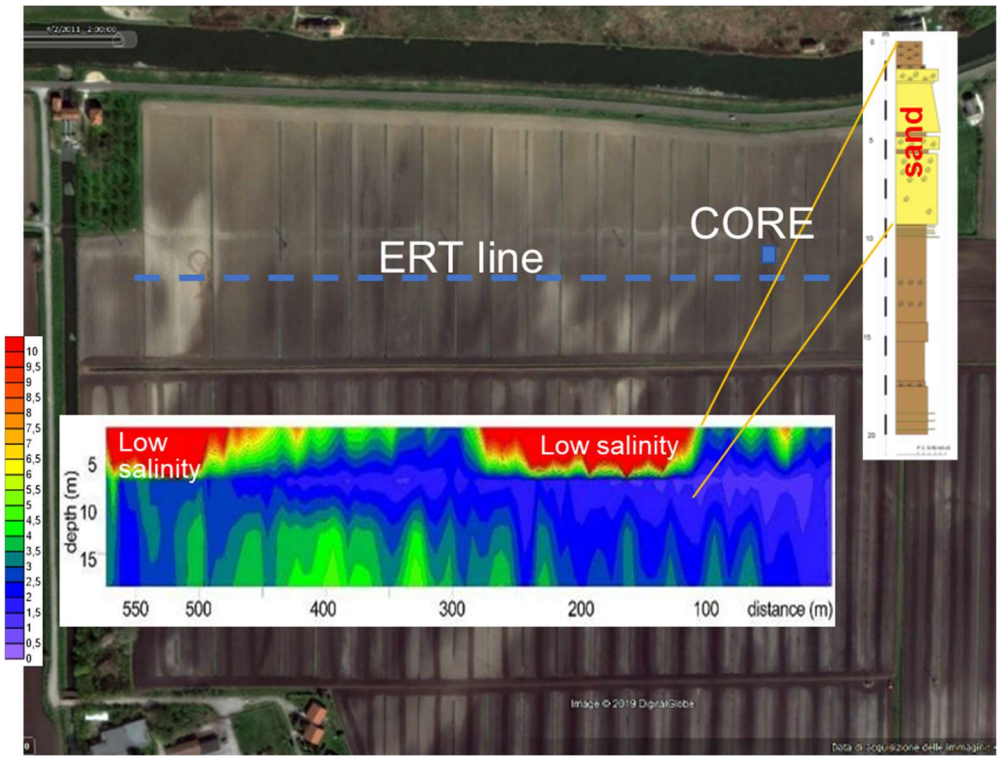

Fig. 18 - *ERT and sediment core used for the characterization of the paleochannel.*

Fig. 19 shows the hydrogeological model sketched along a section crossing the pilot test site selected for the implementation of the mitigation measure to reduce salinity in the farmland. Along this section, the subsoil shows two main quite uniform units consisting in an upper sandy body about 10 m thick and a lower unit, mostly formed by silty sand and silty clay layers. The over-consolidated clay known as caranto lies at about 17 m below msl. The top of the paleosoil marks the boundary between uppermost Pleistocene alluvial sedimentation and, above it, the Holocene units, formed by marine-lagoon and back barrier deposits.

EC logs, recorded along the same cross section, show a high spatial variability of the saltwater presence in the shallow aquifer system (well S1 and S3) as well as the variability of the water column in the watercourses.

Although the continuity of the sandy geomorphological body toward the lagoon basin is not yet proved, on the basis of the water levels of the Morto channel, Bacchiglione and Brenta rivers, the subsoil setting and the ground elevation of the farmlands and riverbeds, the aquifer contained in the sandy body is expected to be influenced by the watercourses.

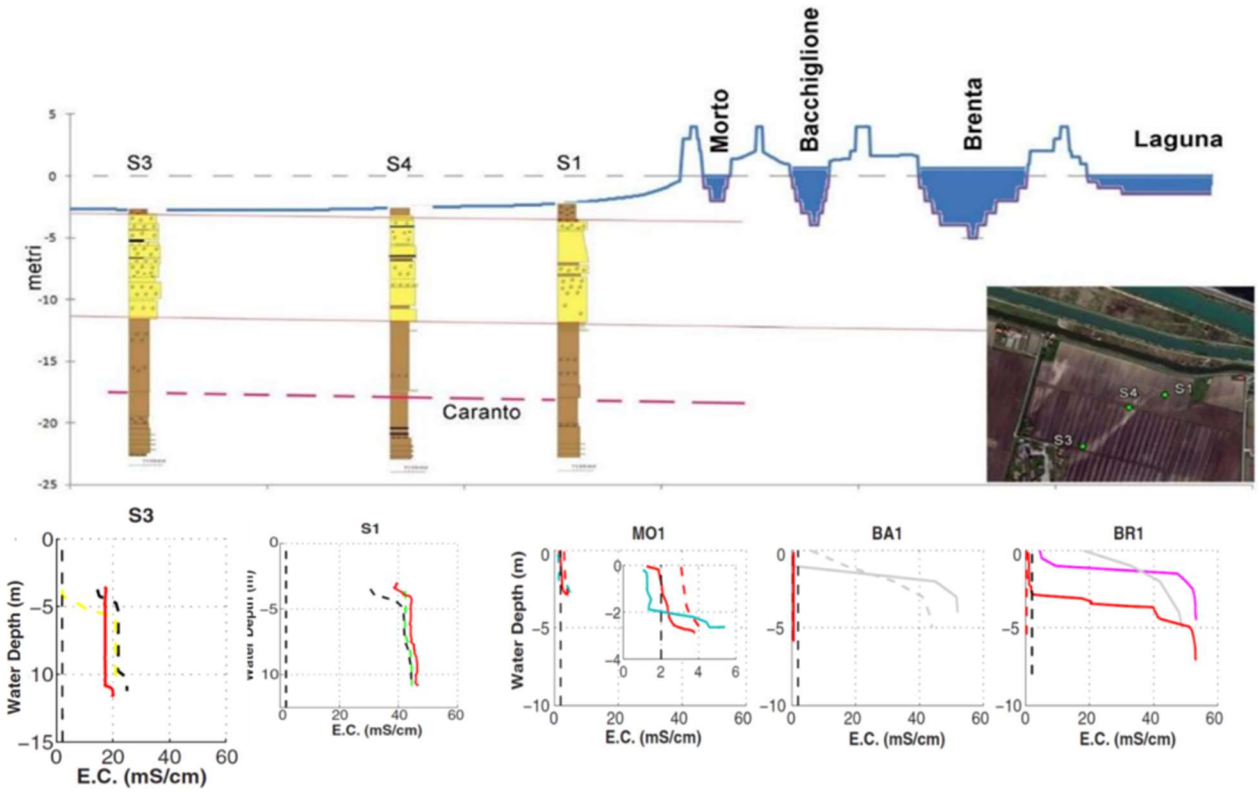

Fig. 19 - *Hydrogeological model along a N-S the ground elevation profile of the pilot test site. The dashed line represents the maximum EC value for irrigation use.*

7. Initial hydrogeological conditions of the Italian site

This section reports the state of saltwater contamination for four main seasonal conditions for the 2020, which refer to February, May, June, July, October and november 2020, i.e. winter, spring, summer and autumn seasons, and two seasonal conditions for the 2021 (February and May), i.e., winter and spring (Fig. 21-82). These conditions can be reasonably assumed as those characterizing the MoST pilot area before the implementation of the planned measures to reduce the salinity in the shallow aquifers.

The groundwater monitoring points available in the pilot area for the measurements carried out in February and May 2020 are composed by CA20, CA50, S1, S2, S3, S4, S5 piezometers. In June, July, October and November 2020 and in 2021 the monitoring network was extended with 6 new piezometers, i.e. MoST 1, MoST 1b, MoST 2, MoST 3, MoST 4, and MoST 5.

Fig. 20 - *Groundwater monitoring network available for the measurements carried out in February and May 2020. The interval depth from ground surface refers to the pipe screen.*

The EC profiles recorded in S2, CA20 and CA50 piezometers refers to three different aquifers, phreatic, locally confined and confined aquifers, respectively. S4 and S5, as well as the piezometers MoST 1 and MoST1b, have the pipe screen in correspondence of two different aquifers: the phreatic and locally confined aquifers. Since the positions of these monitoring points are very close to each other, we can assume that they are representative of aquifers lying at different depths in the same site, thus their EC logs have been plotted in the same chart. The other piezometers (S1, S3, MoST2, MoST3, MoST4, MoST5) refers all to the phreatic aquifer in different positions (Fig. 20).

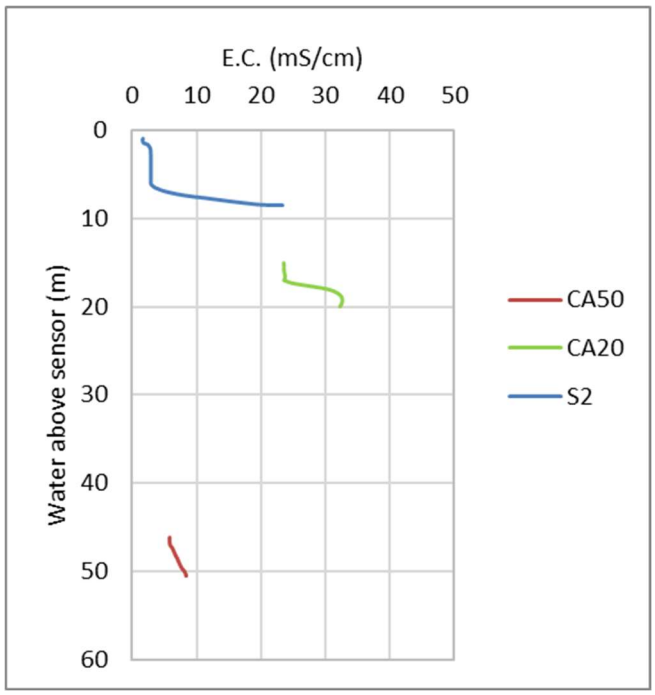

Fig. 21 - *February 2020: EC profile recorded in S2, CA20 and CA50 piezometers.*

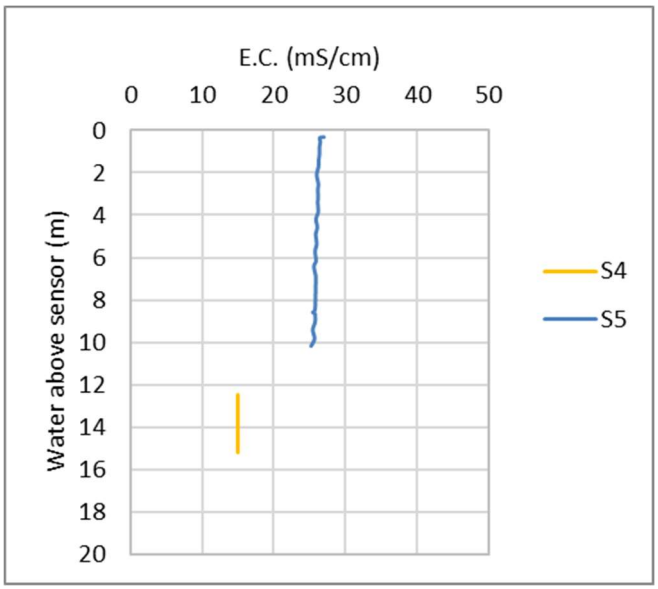

Fig. 22 - *February 2020: EC profile recorded in S4 and S5 piezometers.*

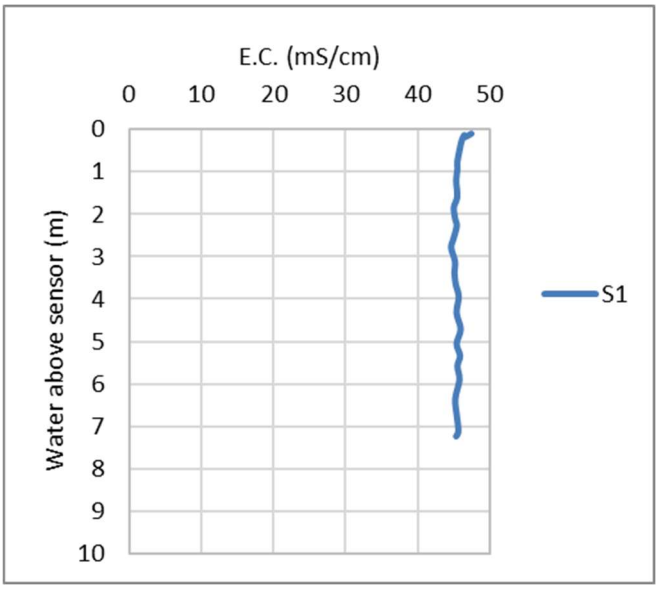

Fig. 23 - *February 2020: EC profile recorded in S1 piezometer.*

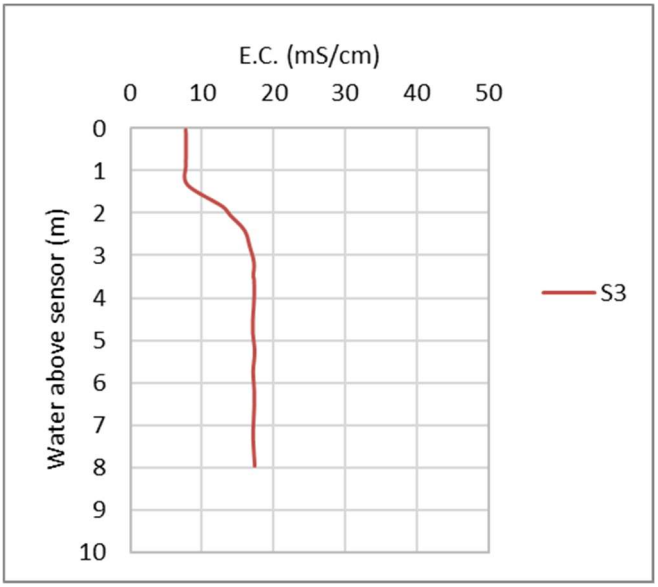

Fig. 24 - *February 2020: EC profile recorded in S3 piezometer.*

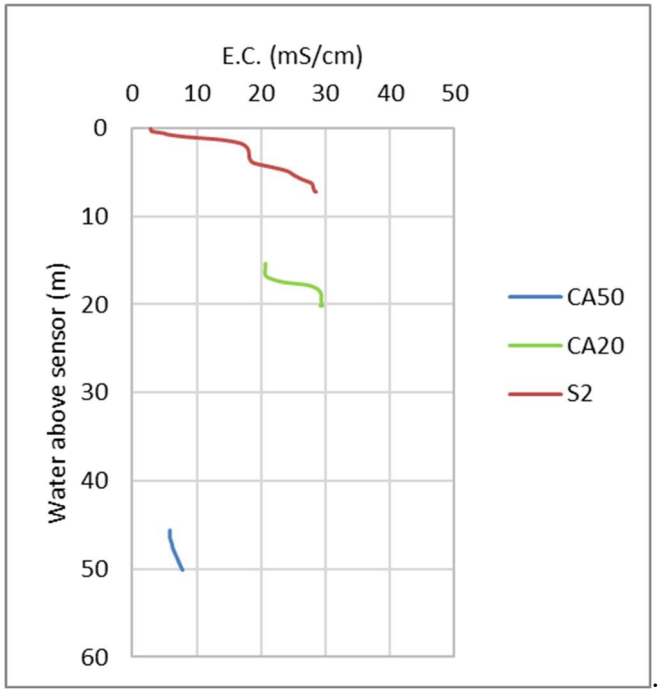

Fig. 25 - *May 2020: EC profile recorded in S2, CA20 and CA50 piezometers.*

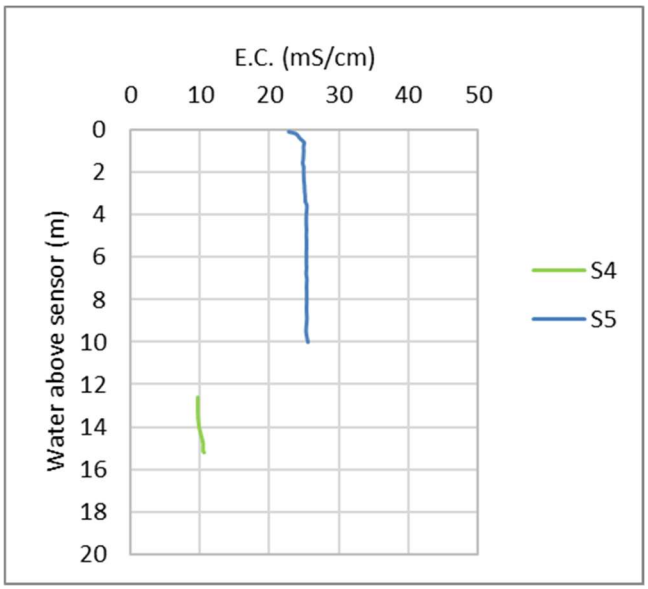

Fig. 26 - *May 2020: EC profile recorded in S4 and S5 piezometers.*

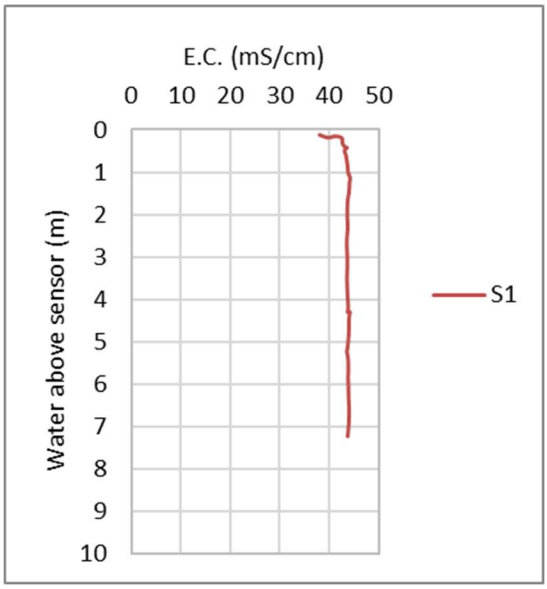

Fig. 27 - *May 2020: EC profile recorded in S1 piezometer.*

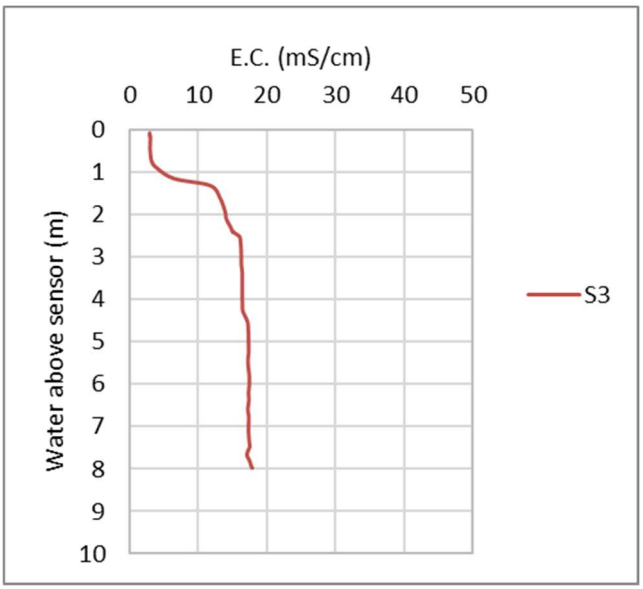

Fig. 28 - *May 2020: EC profile recorded in S3 piezometer.*

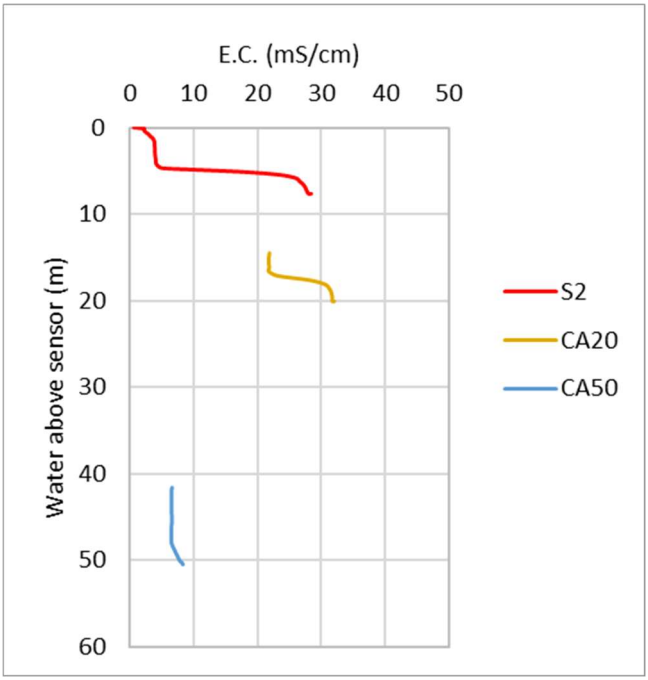

Fig. 29 - *June 2020: EC profile recorded in S2, CA20 and CA50 piezometers.*

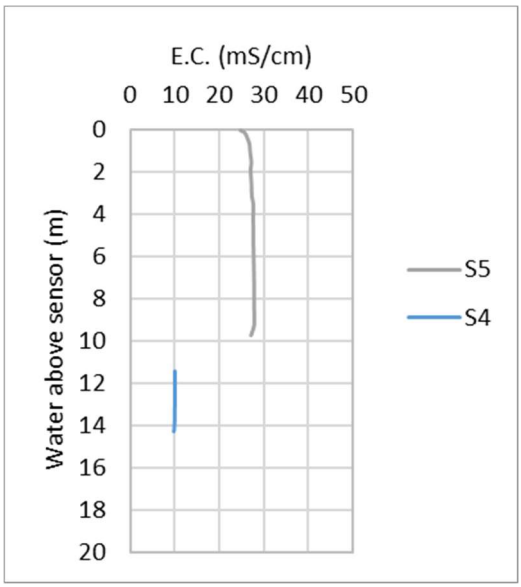

Fig. 30 - *June 2020: EC profile recorded in S4 and S5 piezometers.*

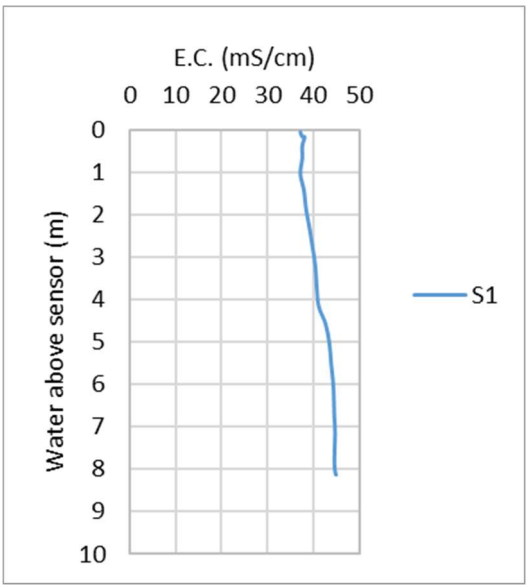

Fig. 31 - *June 2020: EC profile recorded in S1 piezometer.*

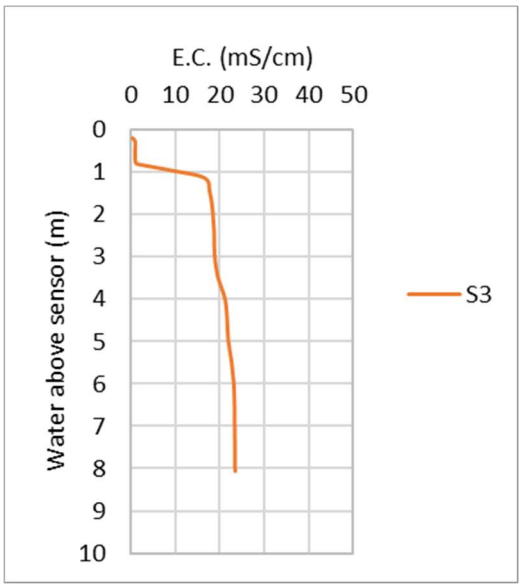

Fig. 32 - *June 2020: EC profile recorded in S3 piezometer.*

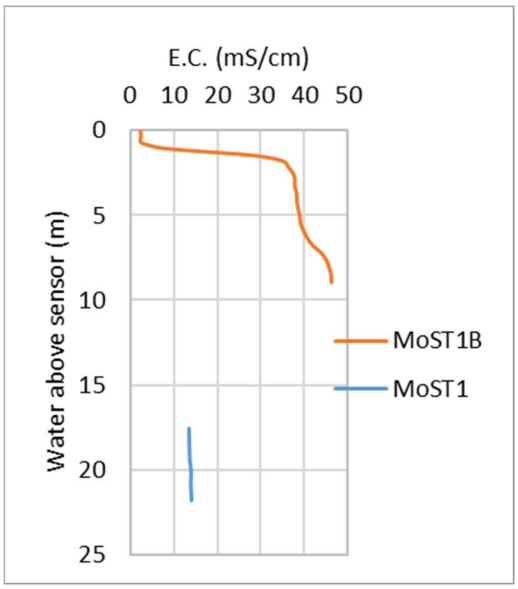

Fig. 33 - *June 2020: EC profile recorded in MoST 1 and MoST1b piezometers.*

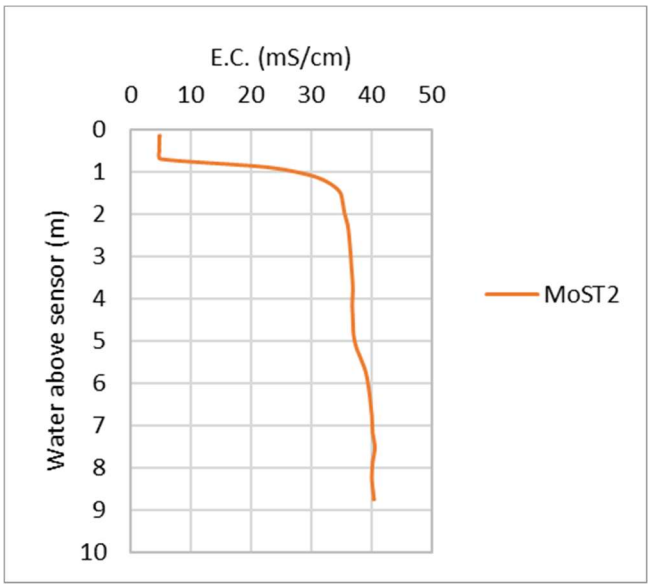

Fig. 34 - *June 2020: EC profile recorded in MoST 2 piezometer.*

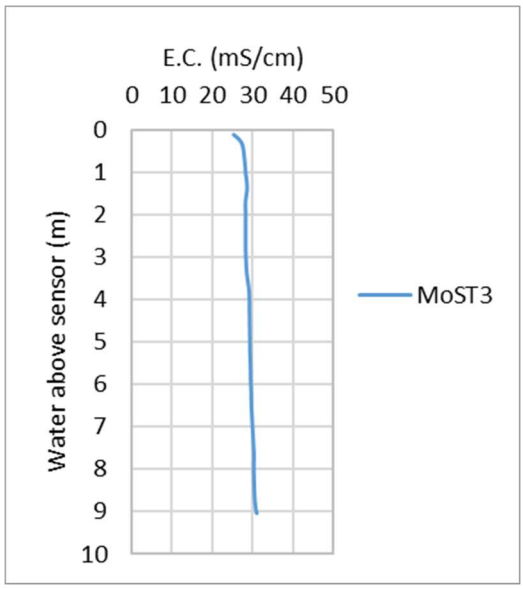

Fig. 35 - *June 2020: EC profile recorded in MoST 3 piezometer.*

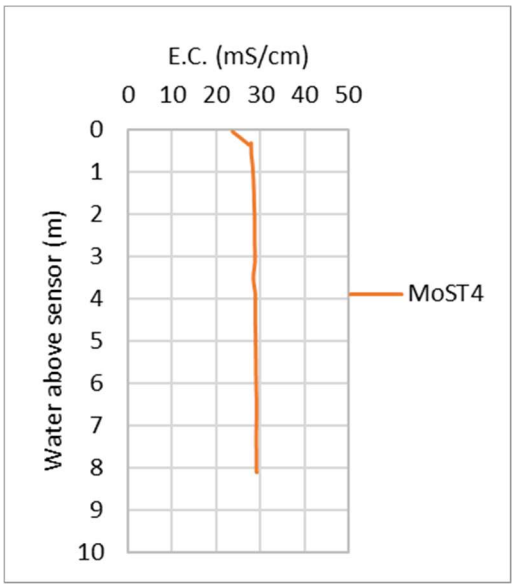

Fig. 36 - *June 2020: EC profile recorded in MoST 4 piezometer.*

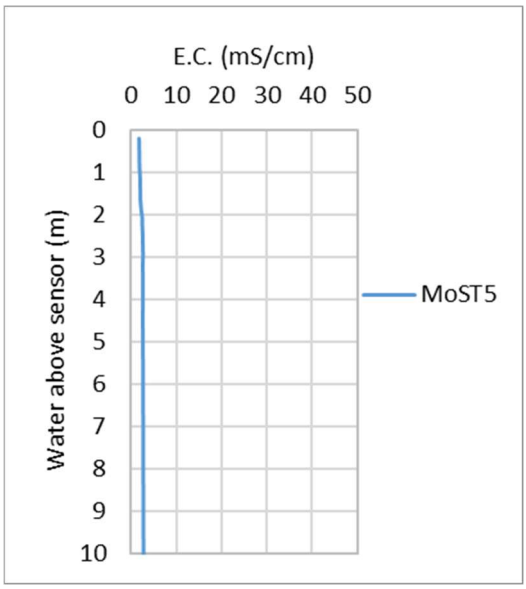

Fig. 37 - *June 2020: EC profile recorded in MoST 5 piezometer.*

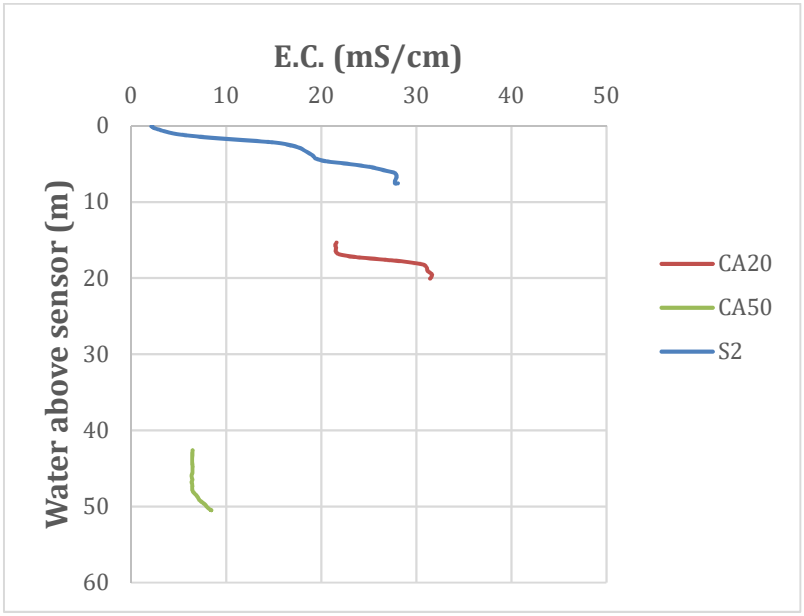

Fig. 38 - *July 2020: EC profile recorded in CA20, CA50 and S2 piezometers*

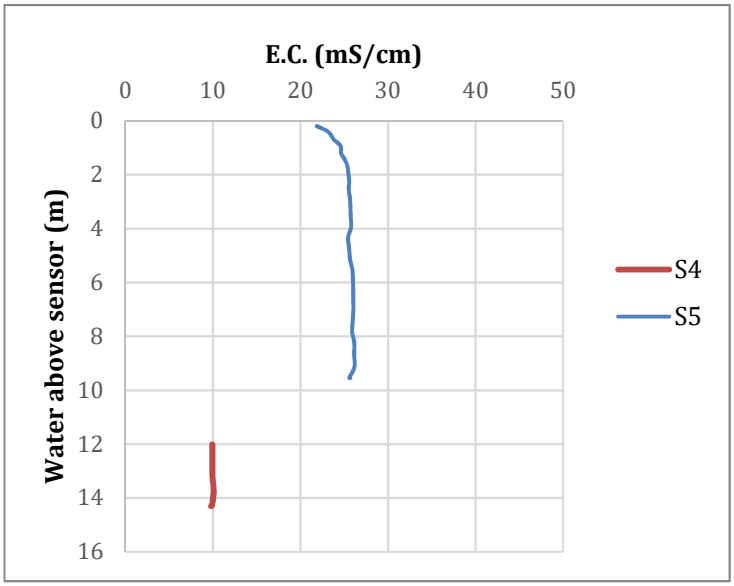

Fig. 39 - *July 2020: EC profile recorded in S4 and S5 piezometers*

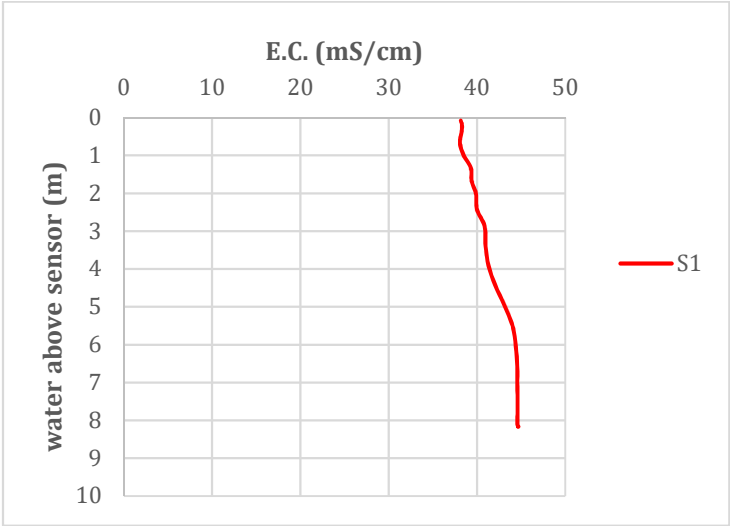

Fig. 40 - *July 2020: EC profile recorded in S1 piezometer*

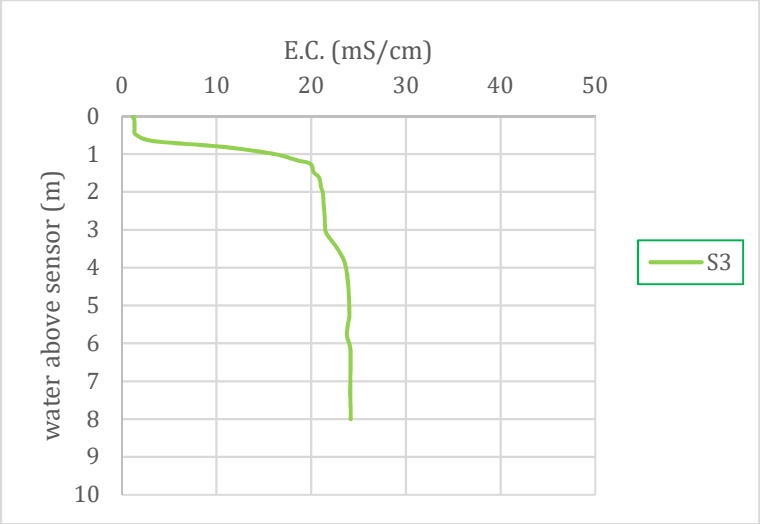

Fig. 41 - *July 2020: EC profile recorded in S3 piezometer*

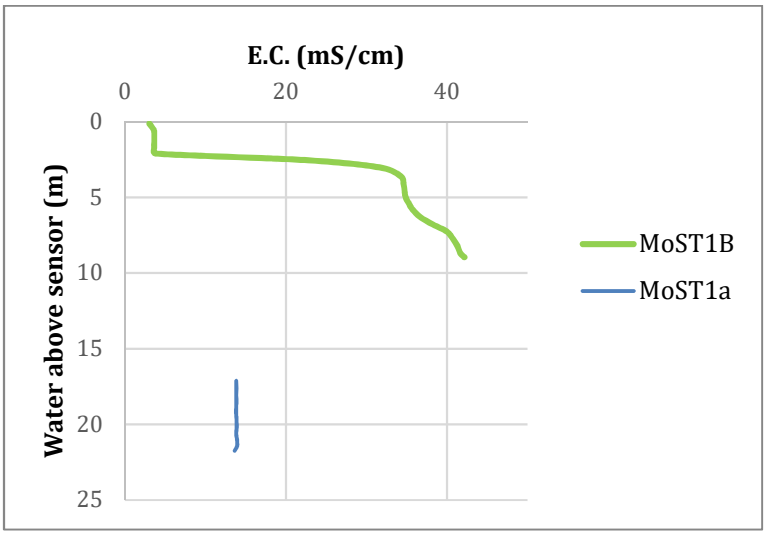

Fig. 42 - *July 2020: EC profile recorded in MoST1a and MoST1b piezometers*

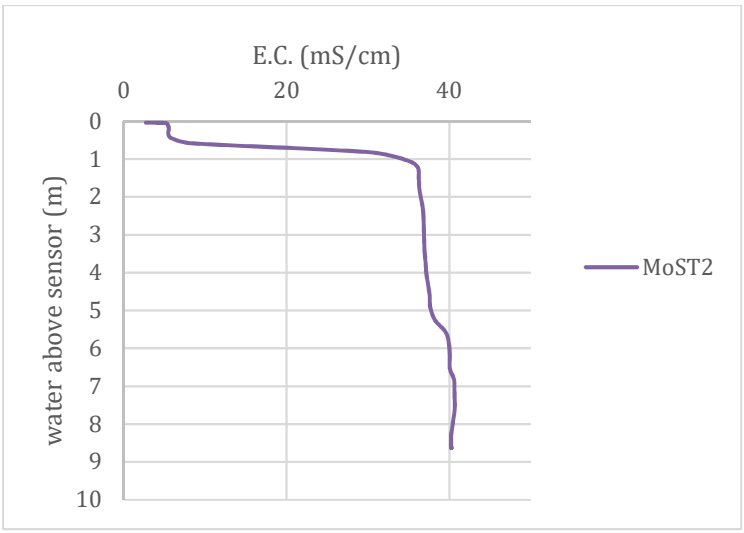

Fig. 43 - *July 2020: EC profile recorded in MoST2 piezometer*

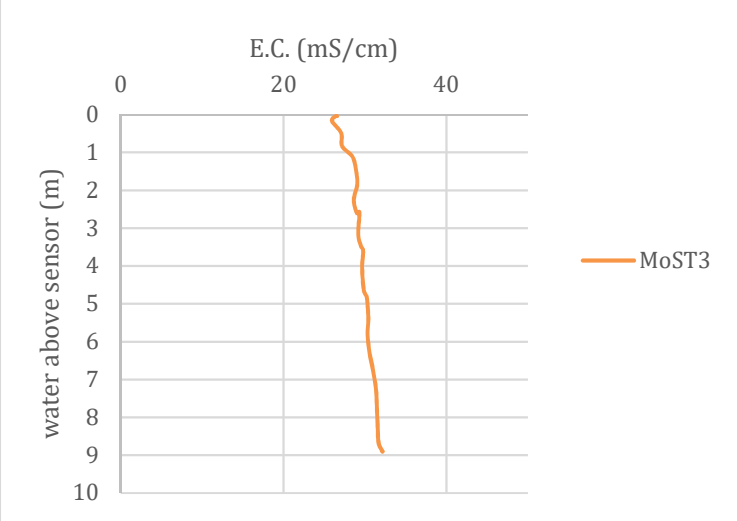

Fig. 44 - *July 2020: EC profile recorded in MoST3 piezometer*

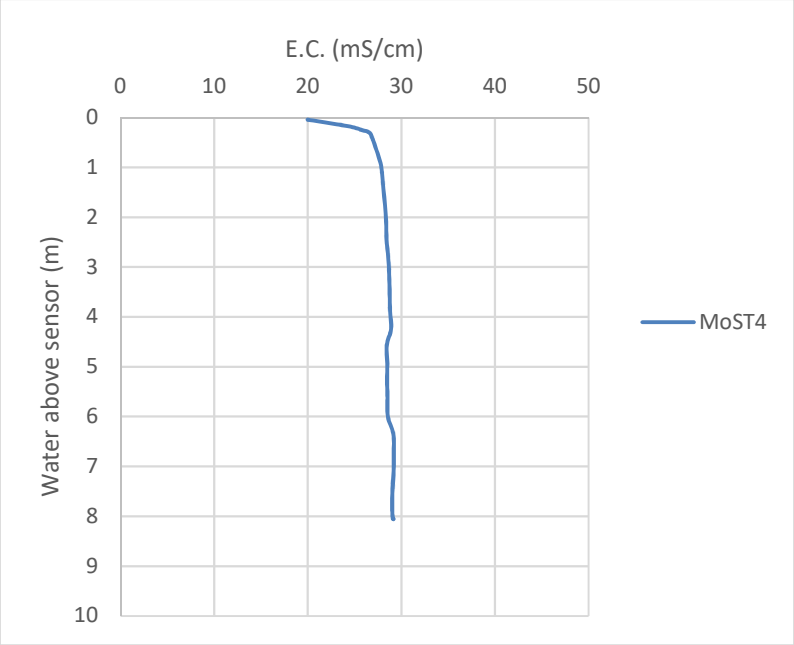

Fig. 45 - *July 2020: EC profile recorded in MoST4 piezometer*

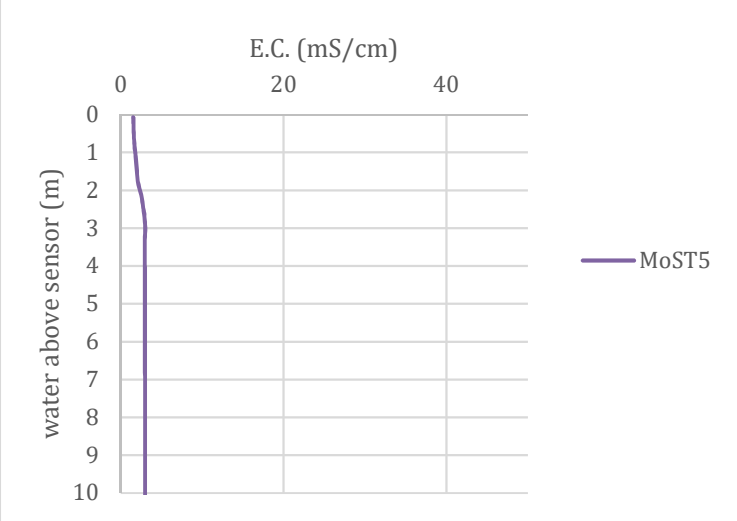

Fig. 46 - *July 2020: EC profile recorded in MoST5 piezometer*

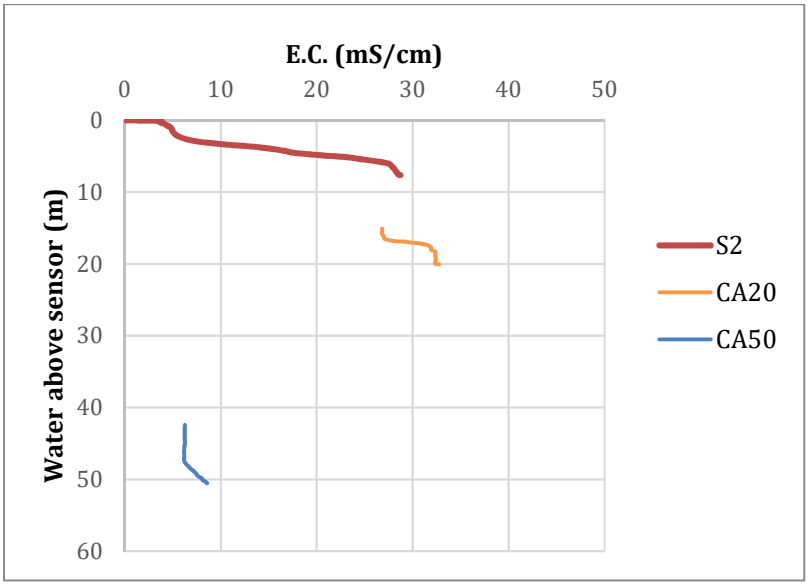

Fig. 47 - *October 2020: EC profile recorded in S2, CA20 and CA50 piezometers*

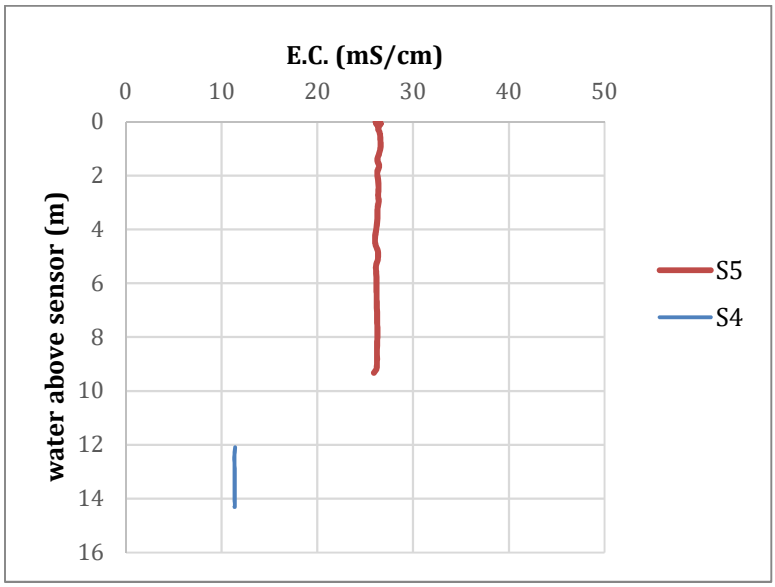

Fig. 48 - *October 2020: EC profile recorded in S4 and S5 piezometers*

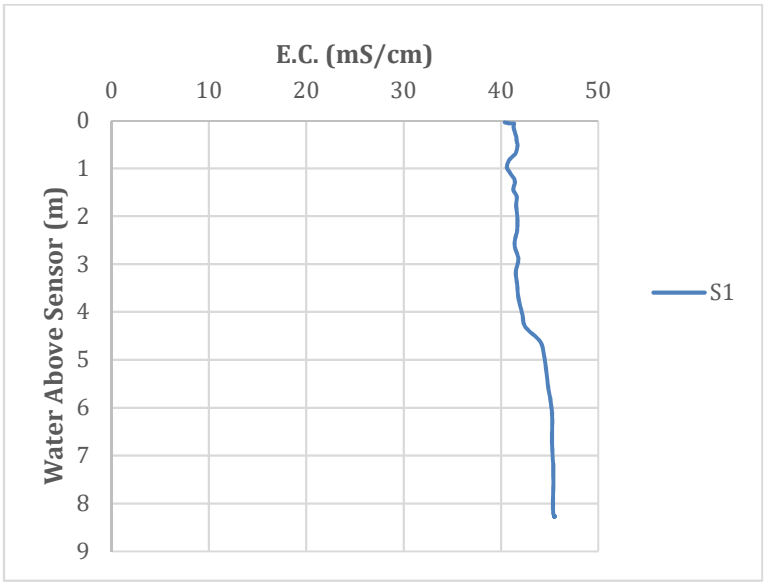

Fig. 49 - *October 2020: EC profile recorded in S1 piezometer*

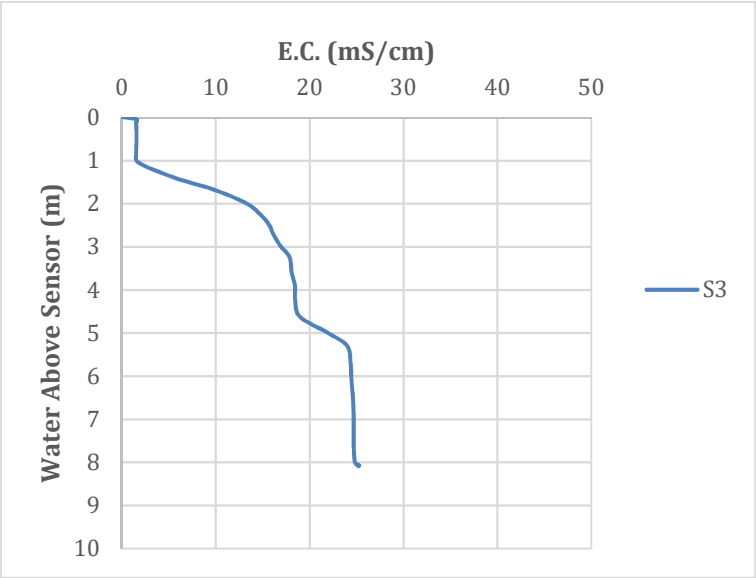

Fig. 50 - *October 2020: EC profile recorded in S3 piezometer*

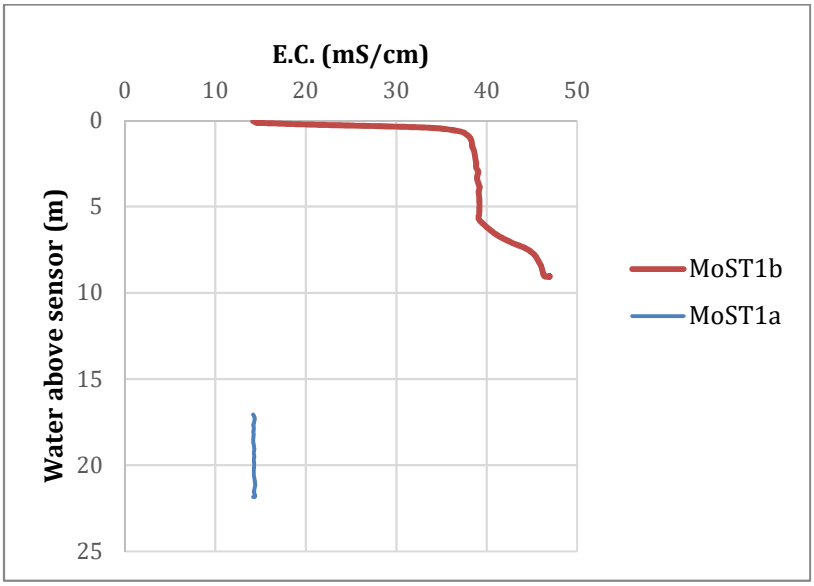

Fig. 51 - *October 2020: EC profile recorded in MoST1a and MoST1b piezometers*

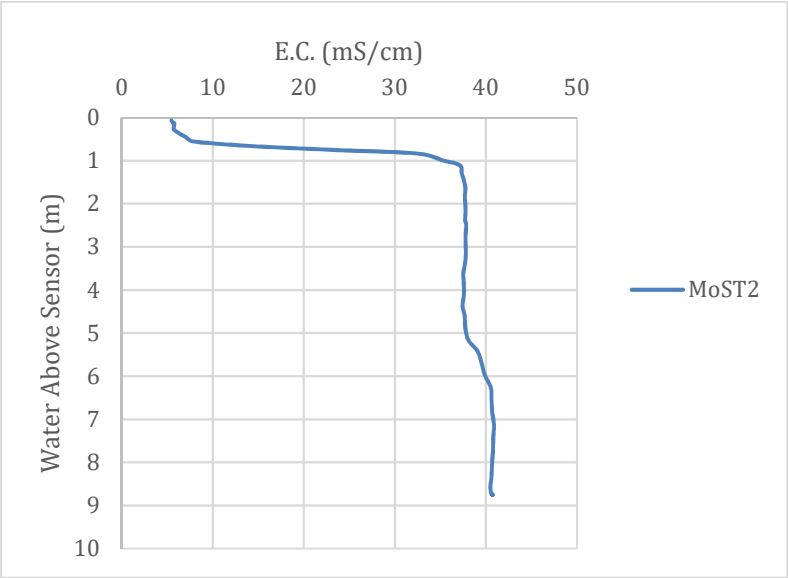

Fig. 52 - *October 2020: EC profile recorded in MoST2 piezometer*

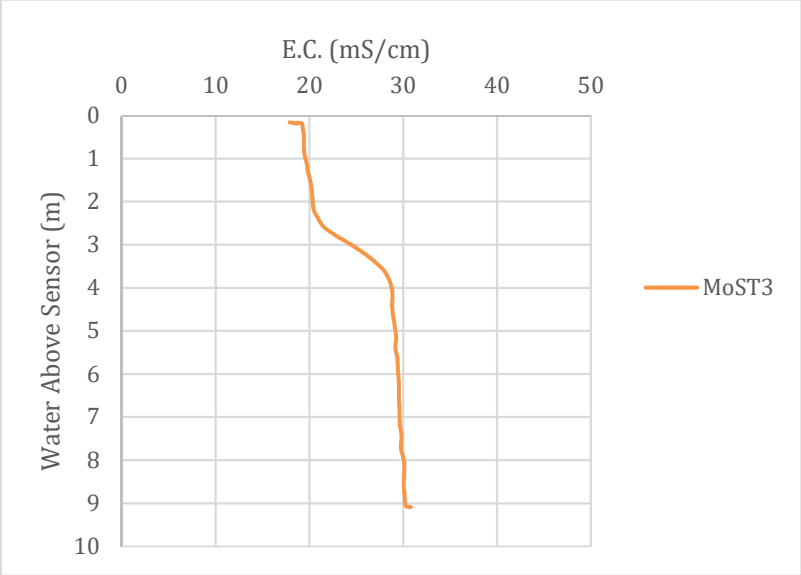

Fig. 53 - *October 2020: EC profile recorded in MoST3 piezometer*

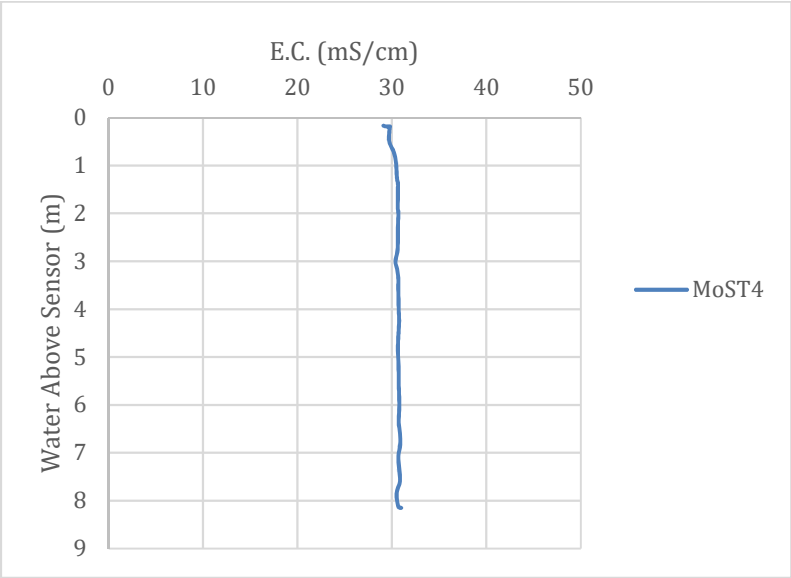

Fig. 54 - *October 2020: EC profile recorded in MoST4 piezometer*

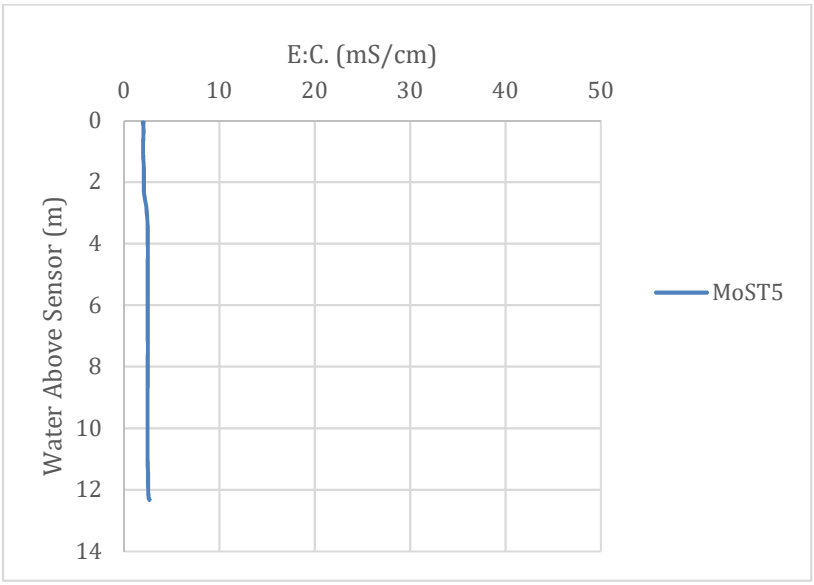

Fig. 55 - *October 2020: EC profile recorded in MoST5 piezometer*

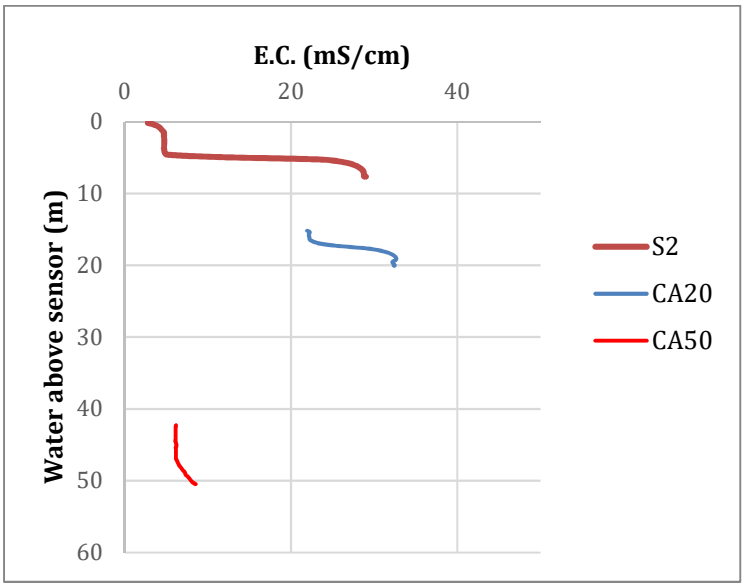

Fig. 56 - *November 2020: EC profile recorded in S2, CA20, CA50 piezometers*

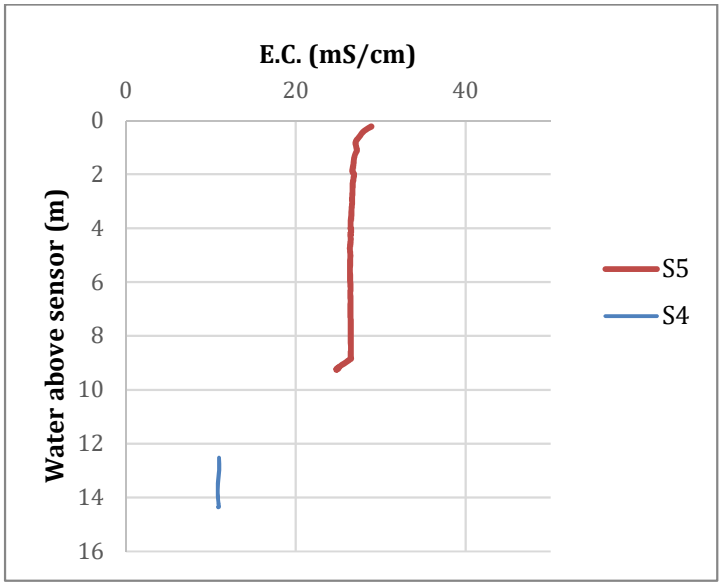

Fig. 57 - *November 2020: EC profile recorded in S5 and S4 piezometers*

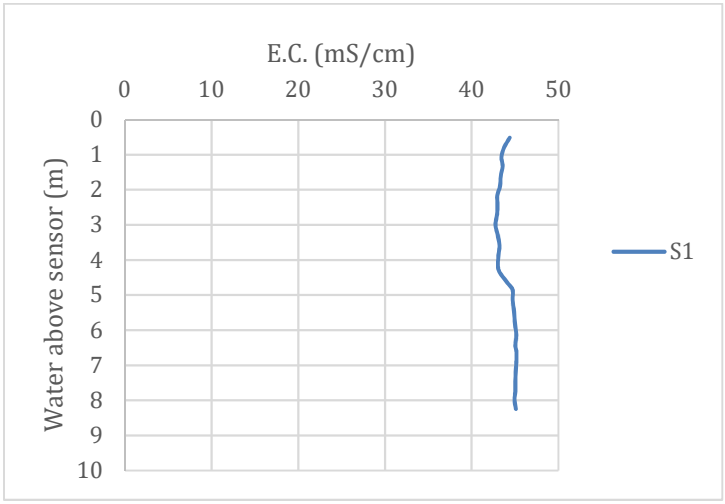

Fig. 58 - *November 2020: EC profile recorded in S1 piezometer*

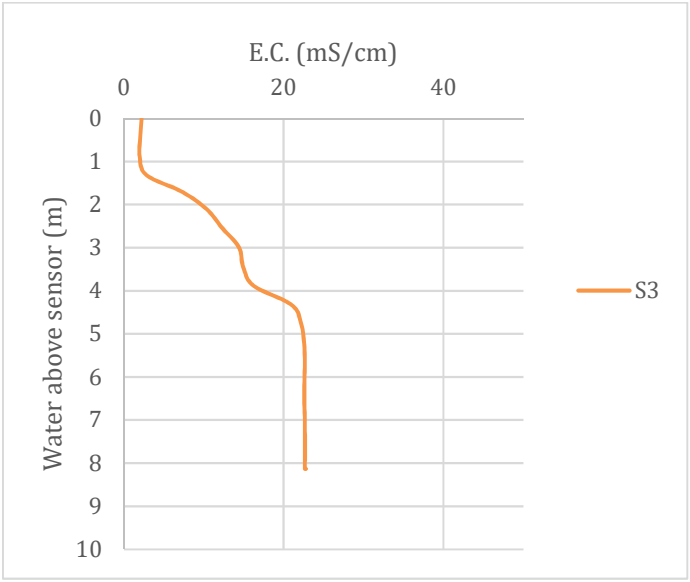

Fig. 59 - *November 2020: EC profile recorded in S3 piezometer*

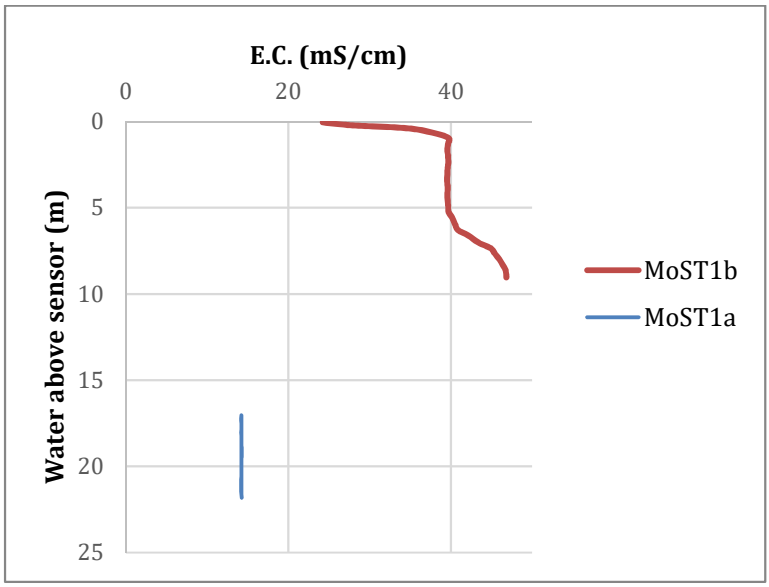

Fig. 60 - *November 2020: EC profile recorded in MoST1a and MoST1b piezometers*

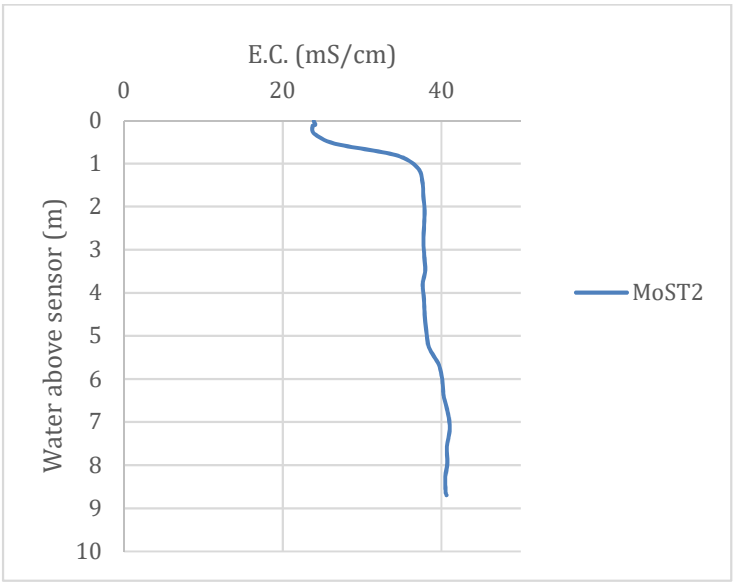

Fig. 61 - *November 2020: EC profile recorded in MoST2 piezometer*

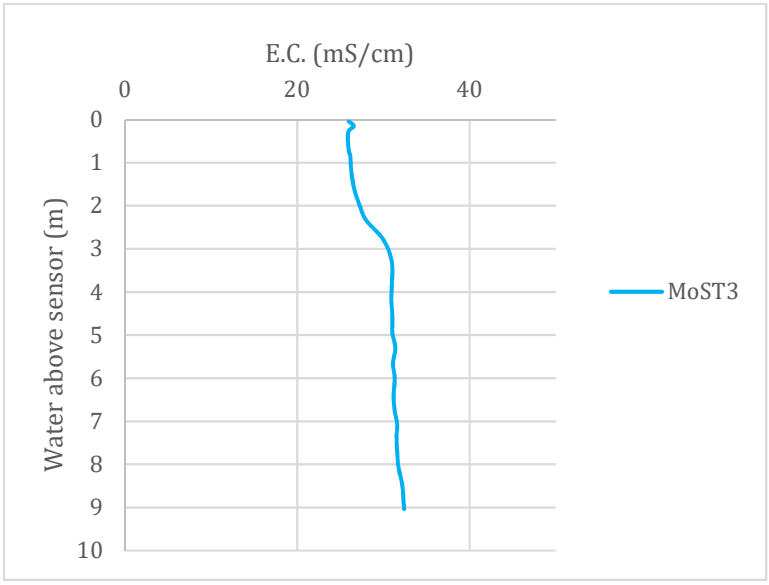

Fig. 62 - *November 2020: EC profile recorded in MoST3 piezometer*

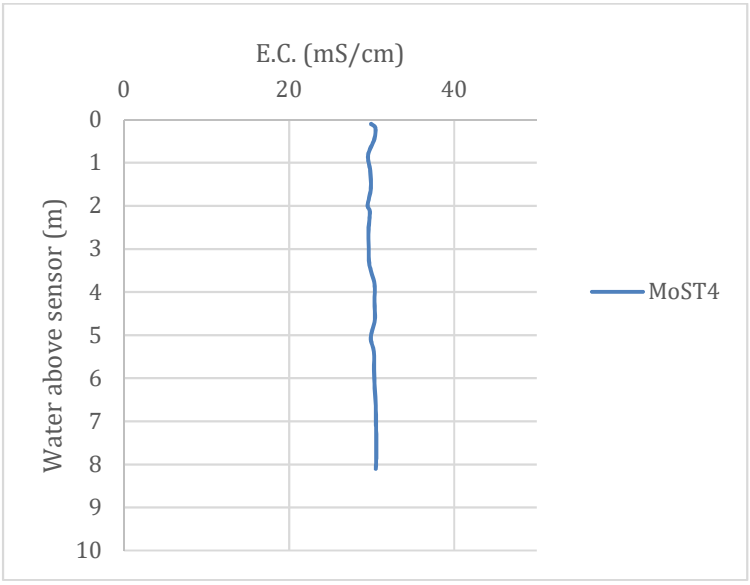

Fig. 63 - *November 2020: EC profile recorded in MoST4 piezometer*

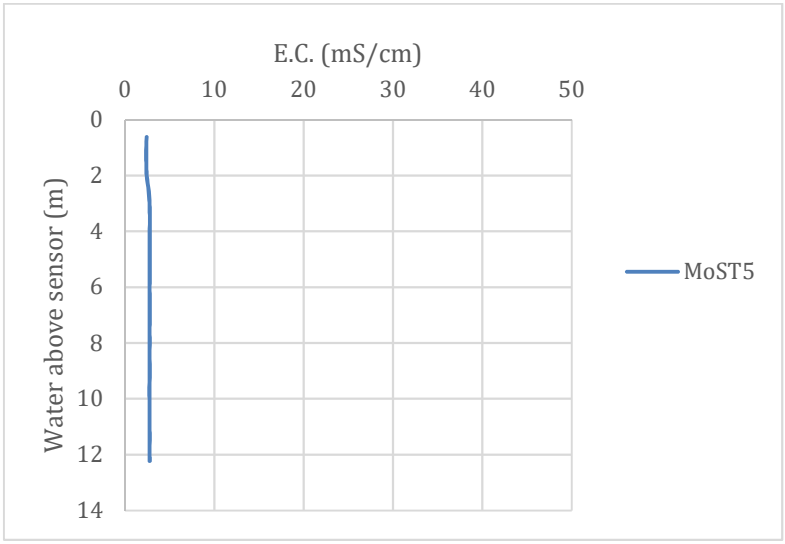

Fig. 64 - *November 2020: EC profile recorded in MoST5 piezometer*

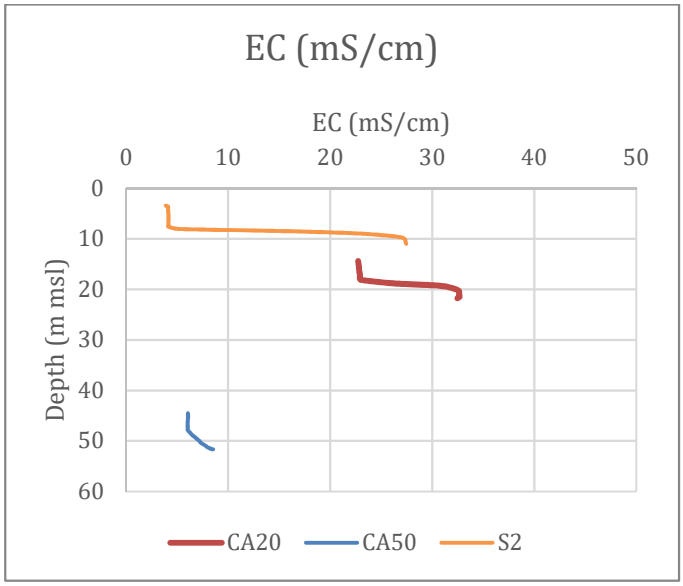

Fig. 65 - February 2021: EC profile recorded in CA50, CA20 and S2 piezometers

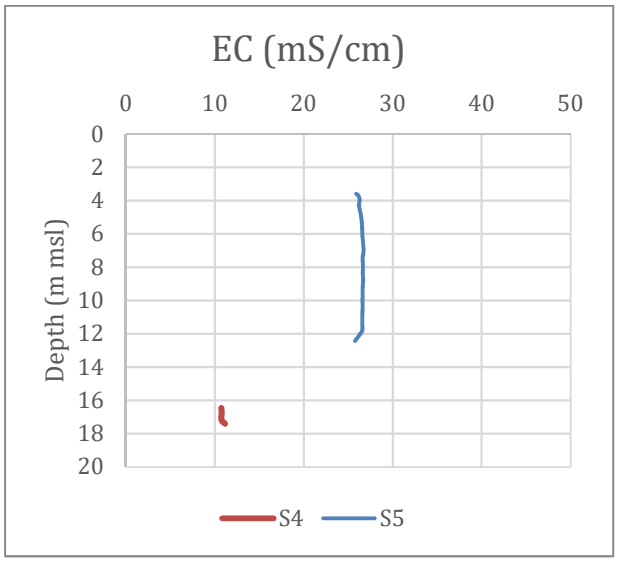

Fig. 66 - February 2021: EC profiles recorded in S4 and S5 piezometers

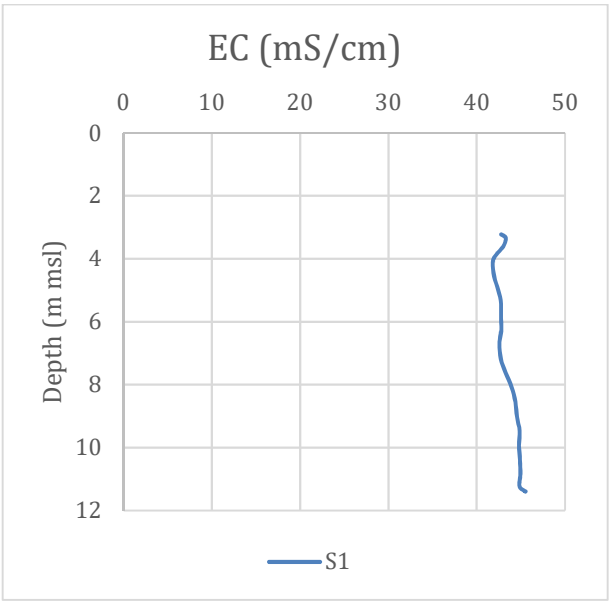

Fig. 67 - February 2021: EC profile recorded in S1 piezometer

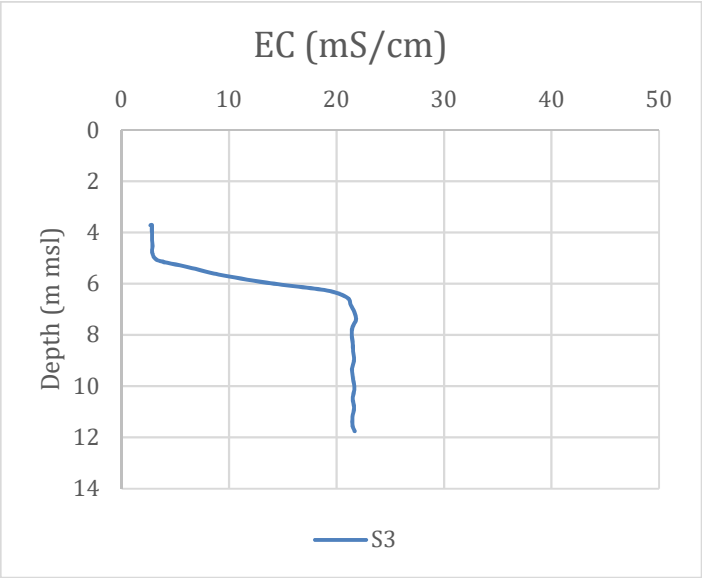

Fig. 68 - February 2021: EC profile recorded in S3 piezometer

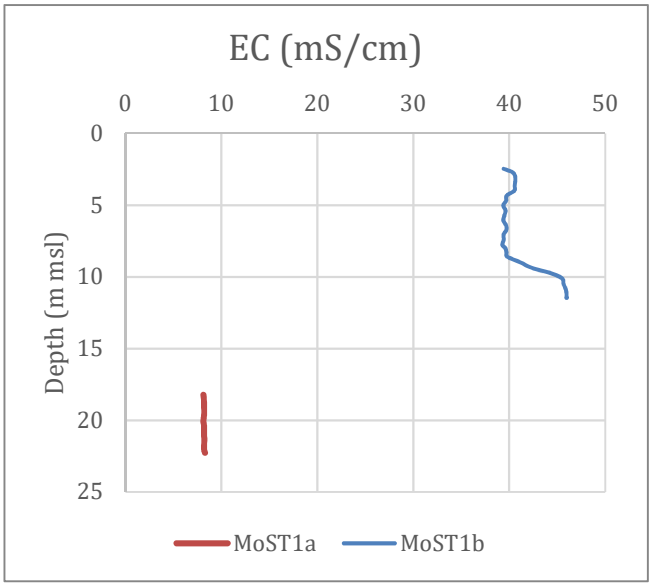

Fig. 69 – February 2021: EC profiles recorded in MoST1a and MoST1b piezometers

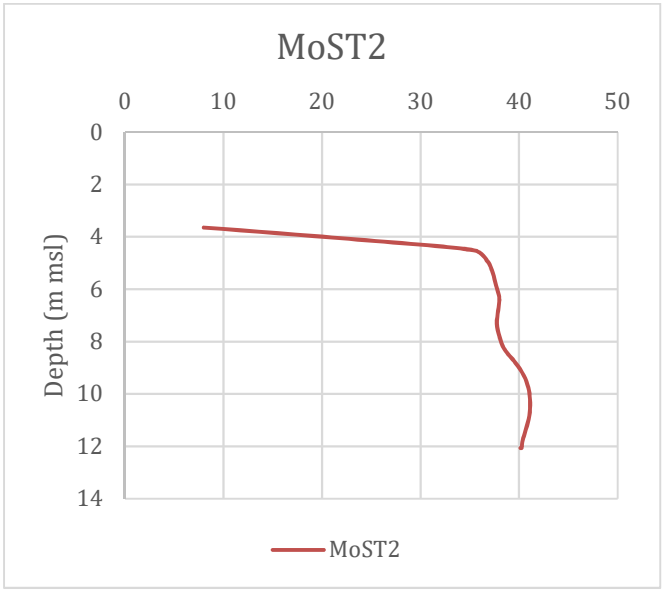

Fig. 70 - February 2021: EC profile recorded in MoST2 piezometer

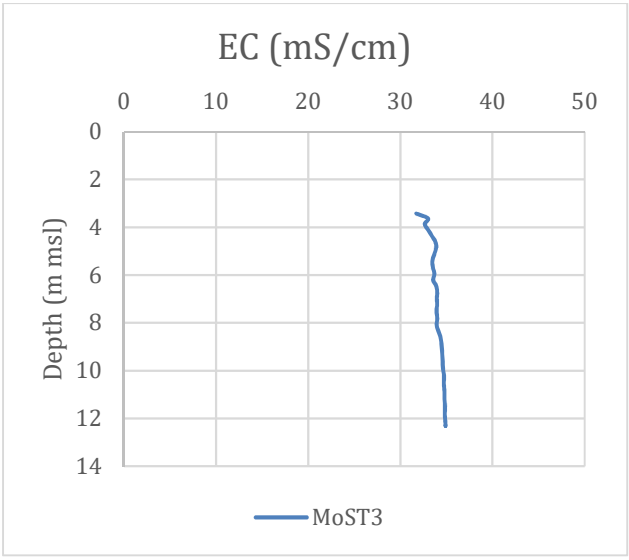

Fig. 71 - February 2021: EC profile recorded in MoST3 piezometer

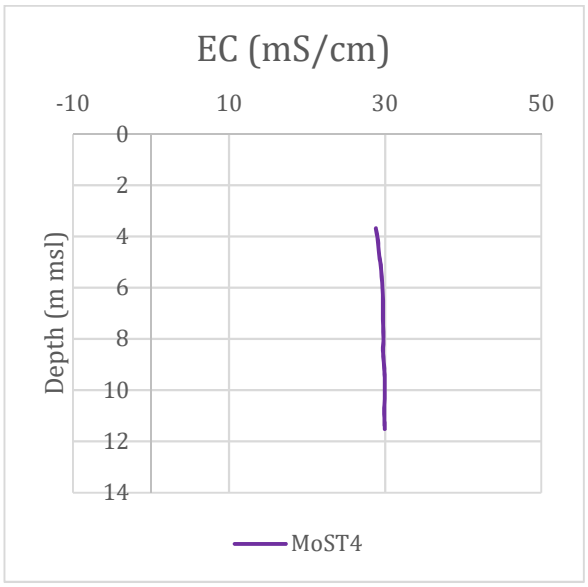

Fig. 72 - February 2021: EC profile recorded in MoST4 piezometer

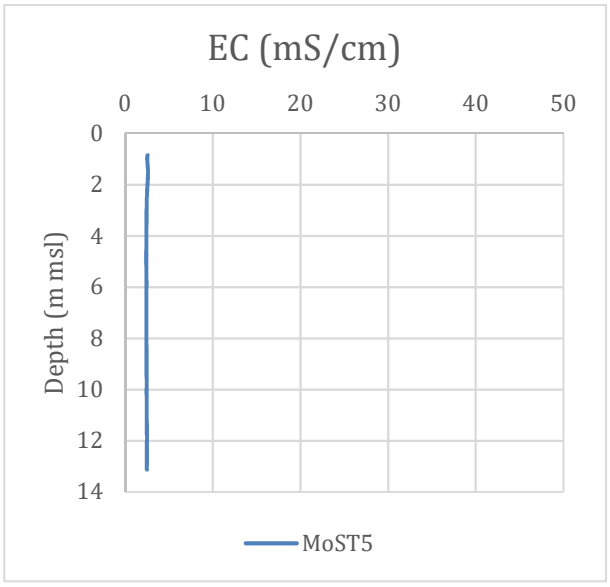

Fig. 73 - February 2021: EC profile recorded in MoST5 piezometer

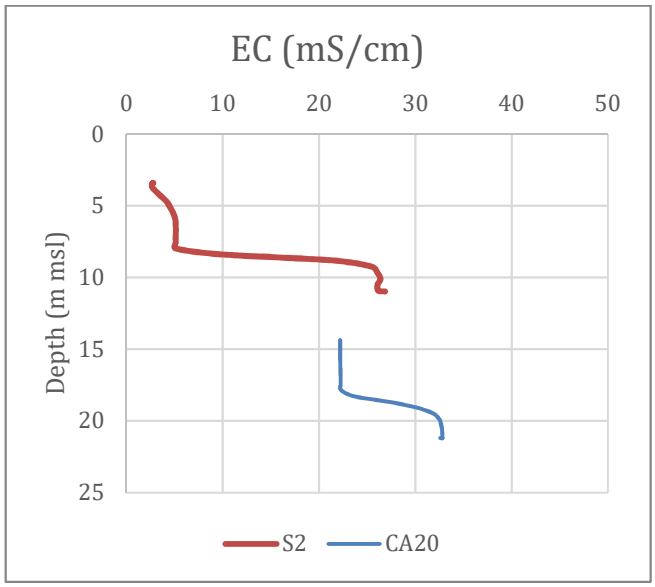

Fig. 74 - May 2021: EC profiles recorded in S2 and CA20

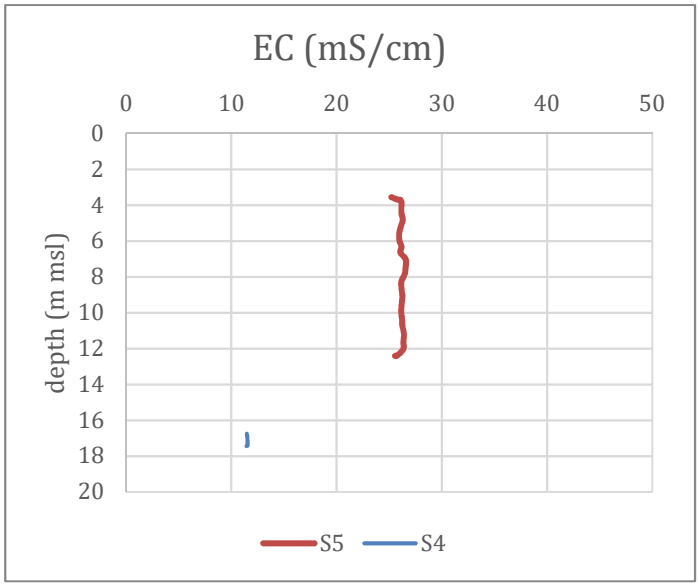

Fig. 75 - May 2021: EC recorded in S5 and S4 piezometers

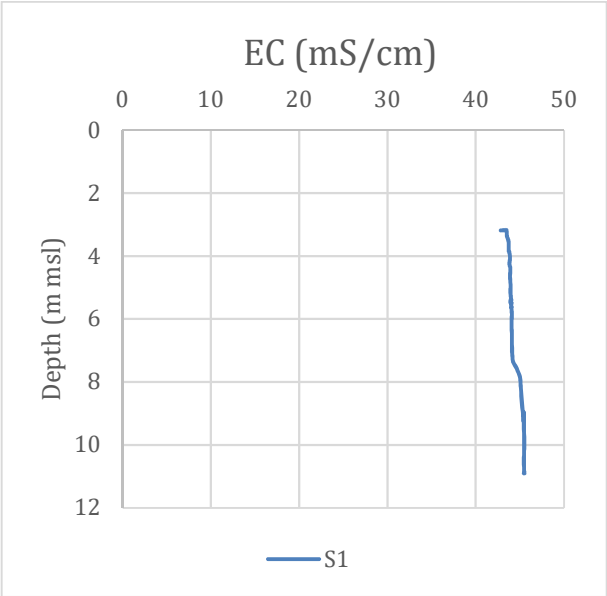

Fig. 76 - May 2021: EC recorded in S1 piezometer

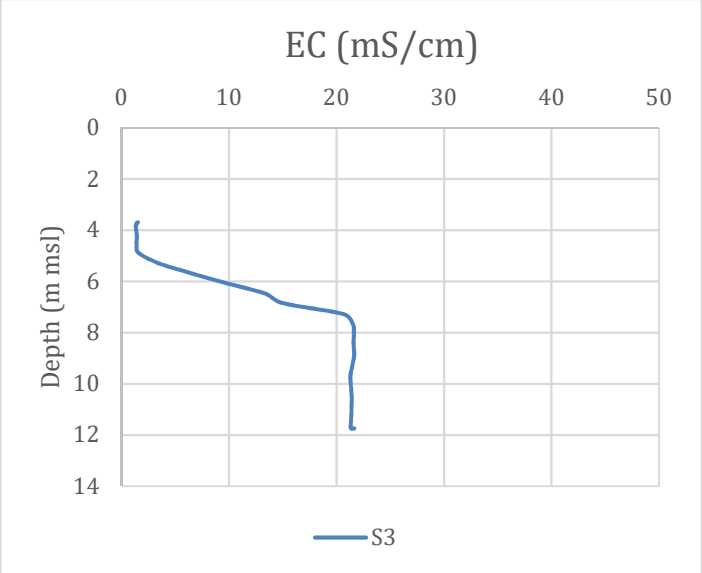

Fig. 77 - May 2021: EC recorded in S3 piezometer

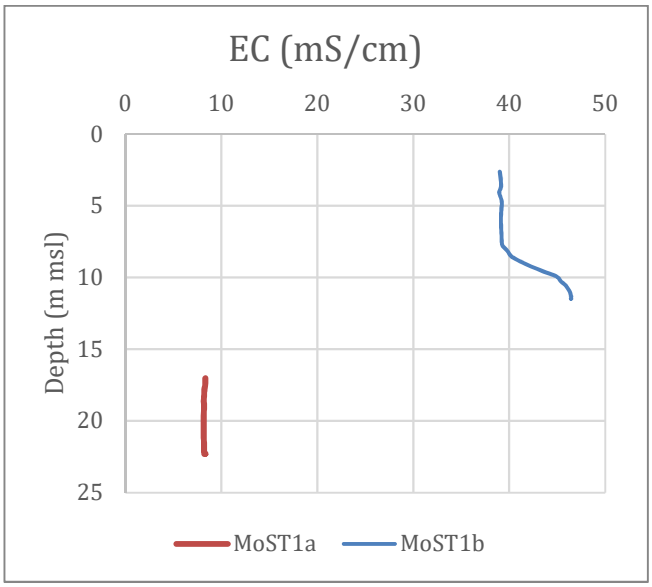

Fig. 78 - May 2021: EC recorded in MoST1a and MoST1b piezometers

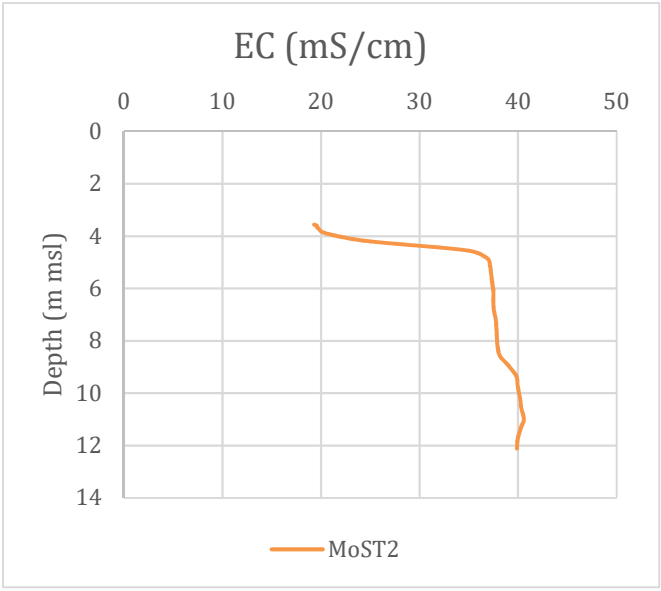

Fig. 79 - May 2021: EC recorded in MoST2 piezometer

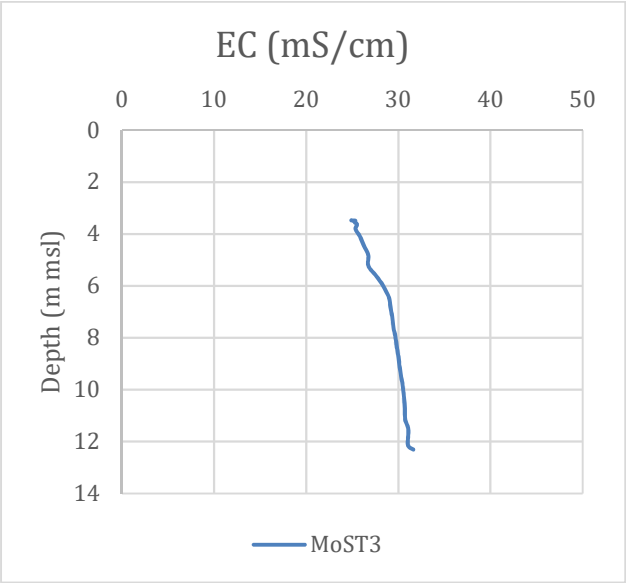

Fig. 80 - May 2021: EC recorded in MoST3 piezometer

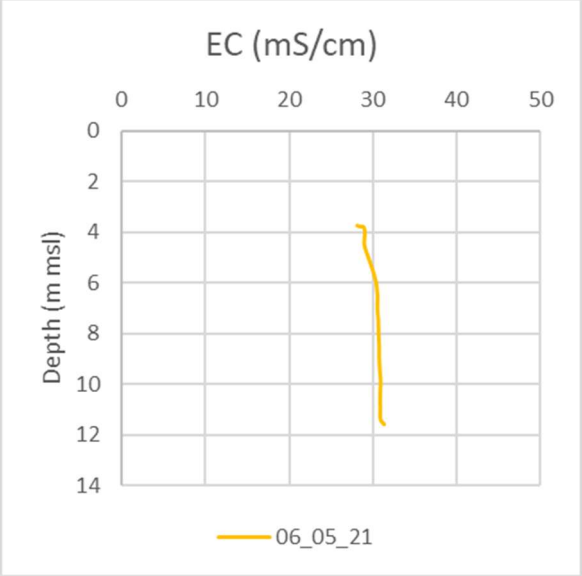

Fig. 81 - May 2021: EC recorded in MoST4 piezometer

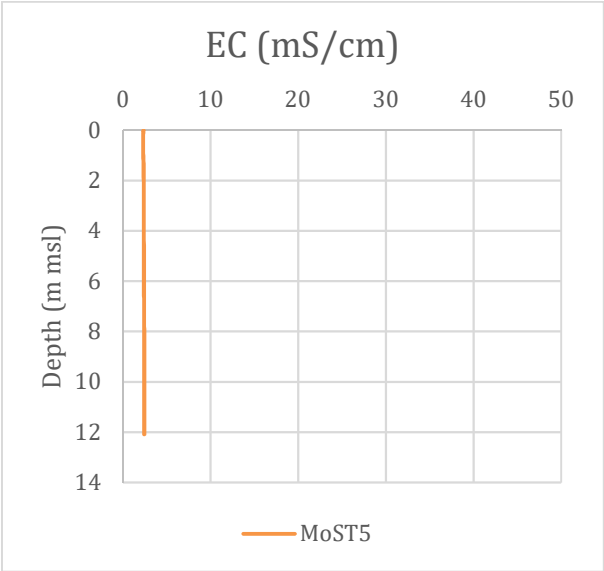

Fig. 82 - May 2021: EC recorded in MoST5 piezometer

8. Forcings

In this section, the main forcings - such as precipitation sea level, Canal Morto and drainage channel levels - potentially controlling the groundwater dynamics and the data recorded in the shallow locally confined and phreatic aquifers are analyzed.

The precipitation regime is characterized by sporadic and quite intense short-term precipitations in July and August, which increases in both frequency and amount in mid-September-October, with some peaks typical of the extreme conditions for this region (Fig. 83). Tide Gauge (TG) time series shows the semidiurnal cycle, characteristics of the Adriatic Sea with an approximate maximum

amplitude of 1 m and a slightly increasing trend towards the fall season. The Canal Morto (CM) h value follows that of the sea but with the higher levels significantly reduced by tide TG located at the confluence of the canal with Bacchiglione-Brenta river system. The flow in the canal is in fact strongly dependent of the passive action of TG which, in turn, depends on the interaction of the water levels in the different part the hydraulic node i.e.: stage/discharge in the two rivers, tidal excursion and pumping operations in the reclaimed land. To note that when heavy precipitation and irrigation practices maintain a high h value in the channel, its flow prevails on the tidal ingression and the TG closure can be delayed until the tide level is sufficiently high to drive an upstream current that closes the gates. Slight differences in timing between the changes of water levels of the CM and the sea also depend on the distance between the measuring stations.

The Drainage Channel (DC) is located at a lower ground level with respect to the watercourses that naturally flow into the sea (i.e. the Brenta-Bacchiglione-Canal Morto system). It collects the surface water from the drainage ditches of the area and its maximum and minimum levels are controlled by the Casetta Pumping Station (PS) in a range of levels determined by the requirements of irrigation and agricultural practices. Specifically, the drainage level was increased of 10 cm in July in order to keep water table high to sustain the crop production, while it was decreased of 20 cm at the end of the harvesting, in September. In addition, a temporary reduction of the drainage levels is imposed when heavy precipitation is forecasted, e.g., during the heavy precipitation that occurred in early August. It is important to highlight the behaviour of the h of the drainage channel, which shows higher frequency oscillations in July when amplitude is lower, and vice versa in September and October. To note in mid-October, the recorded temporary increase in the frequency of the water level oscillations in the drainage channel is due to the need to evacuate larger volumes of water from farmlands following the heavy rains. EC measured in CM is generally around 1-1.5 mS cm^{-1}, rarely higher and in any case always lower than 3 mS cm^{-1}.

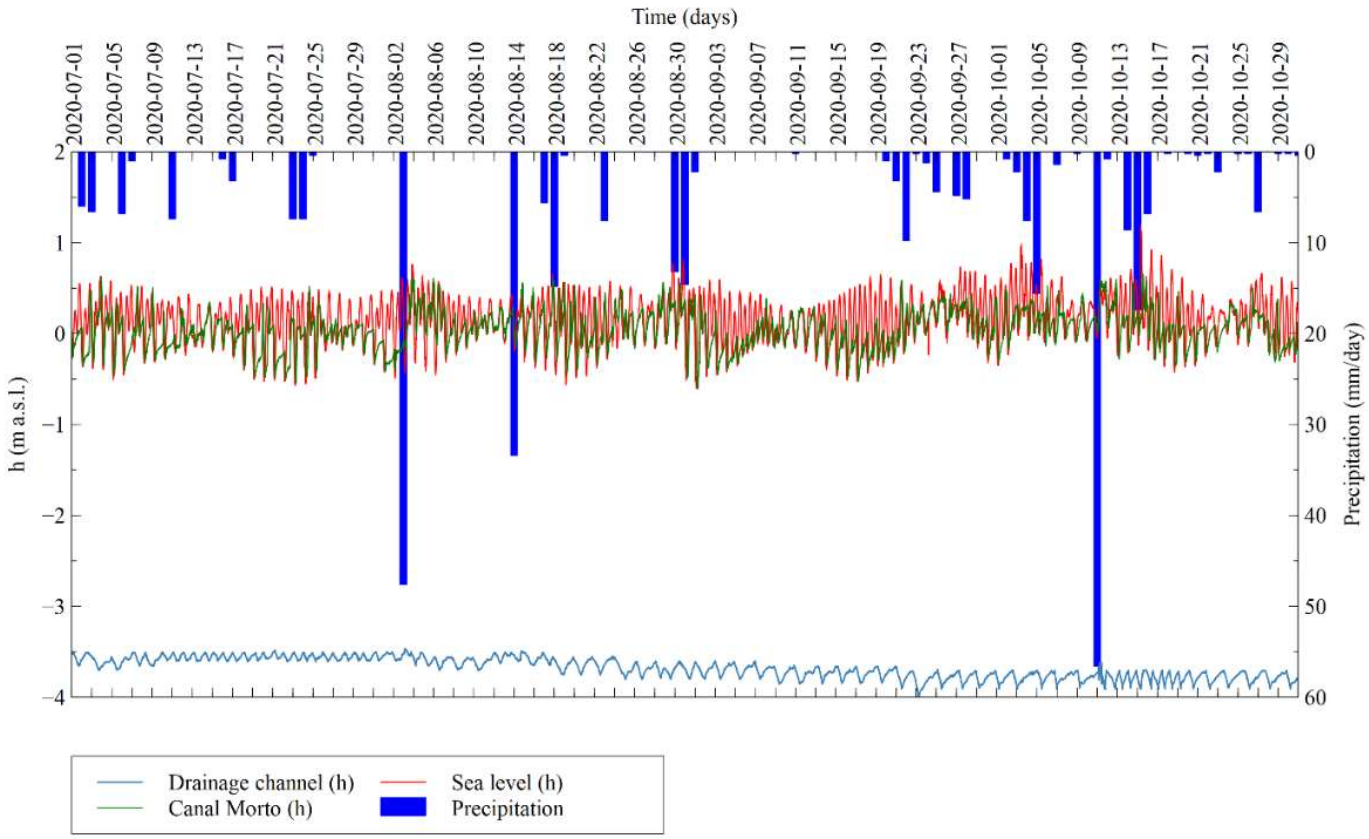

Fig. 83 - Time series of forcing factors of the aquifer dynamics in the southern Venice Lagoon during the period July 1st – October 31st: Daily precipitation from SA meteorological station , Sea level observed at TG; CM water level (PS outflow) and DC h (PS inflow).

Spectral analysis of CM h value highlighted a frequency content dominated by semidiurnal (12 hours 30 minutes) and diurnal (23 hours 40 minutes) periods respectively, while the PS inflow levels exhibited dominant periods of 50-45 hours, the presence of only the diurnal period and the absence of the semidiurnal oscillation. Hence, the CM h values are clearly related to tides while the regulation of the drainage ditch operates as a low-pass filter, cutting the semidiurnal tidal component and introducing a slower varying sawtooth profile on the pumping levels with a period of about 2 days depending on the pump flow rate, the volume of the reservoir and the phreatic aquifer recharge through the leakages (along the CM edges).

Whether data were also hourly acquired by an ATMOS-41 all-in one weather station equipped with a ZL6 datalogger (METER group). Rain and temperature data are shown in Fig. 84.

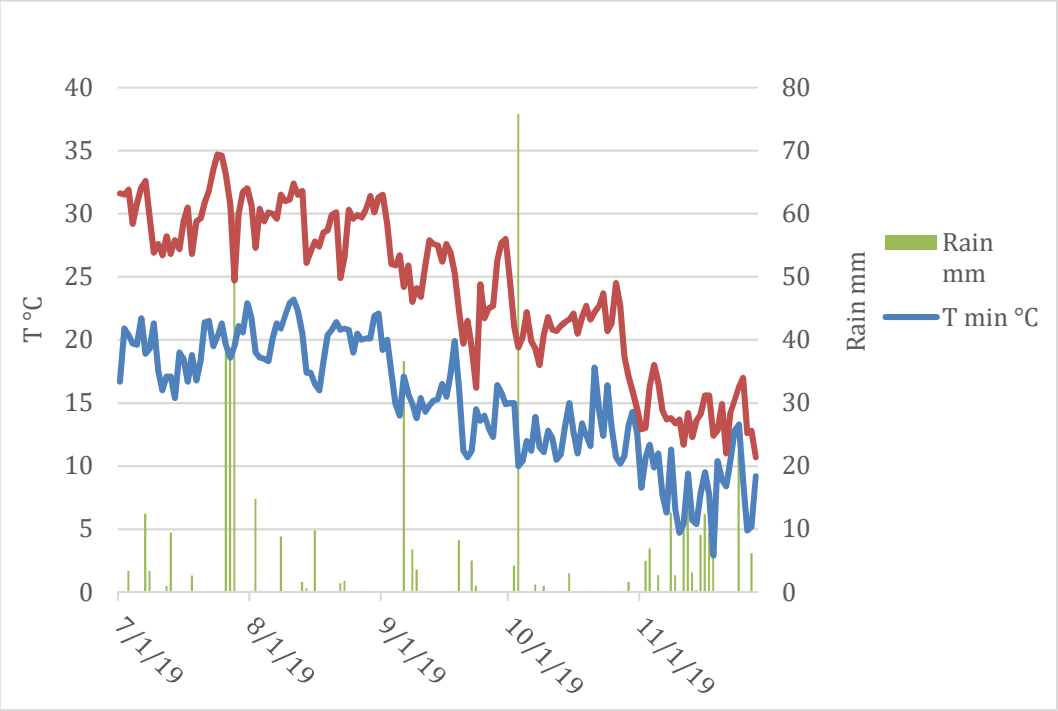

Fig. 84 - Rain and temperature data.

9. Agricultural layer conditions

Five monitoring station were identified (3 inside and 2 outside of the paleochannel) and equipped with one piezometer 2m deep. A sampling campaign was performed from July 2019 until January 2020 at each monitoring station position. It consisted of:

- Water table measurements (once per week)
- Ground water electrical conductivity (EC) measurements (once per week)

Ground water EC (ds/m) and water table depth data (cm below the land surface) are shown in Figure 1 and 2, respectively.

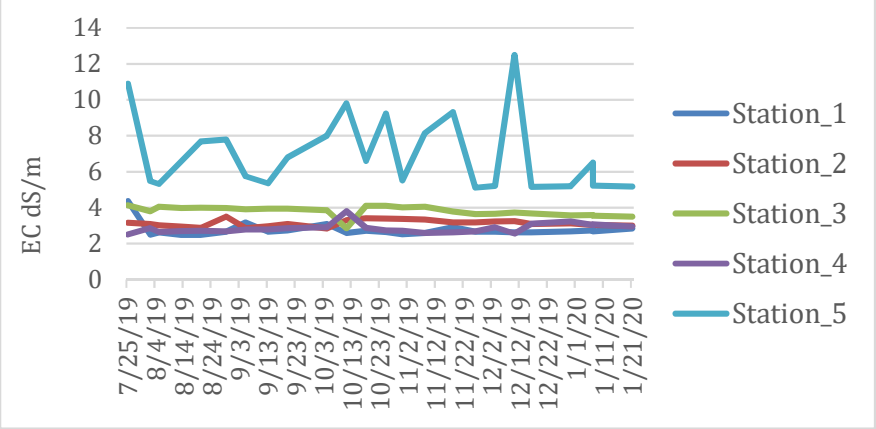

Fig. 85 - Ground water EC data collected at the 5 monitoring stations

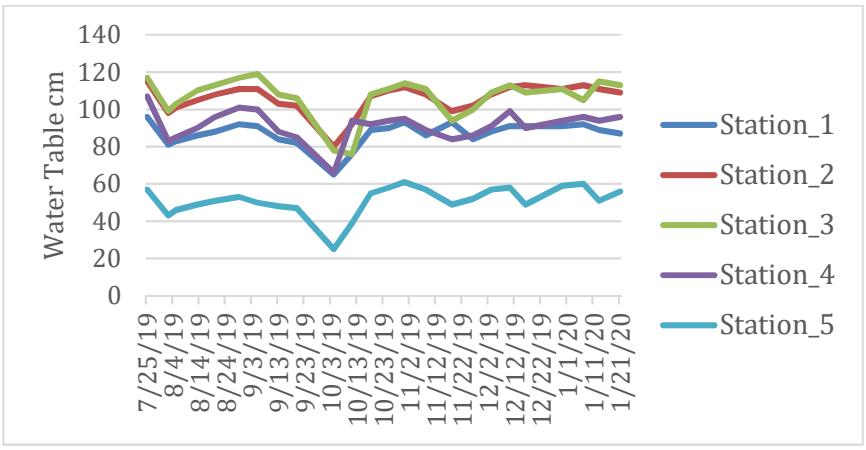

Fig. 86 - Water table depth below the land surface at the 5 monitoring stations

Soil-water monitoring results

Each monitoring station was equipped with 4 soil moisture and electrical conductivity sensors (TEROS 12, METER Group) installed at 4 depths (10. 30, 50 and 70 cm) and 2 or 3 tensiometers (T4e, METER Group) installed at 30, 50 and 70 cm. Electrical conductivity (EC), volumetric water content and matric potential data were hourly collected. Data acquired in two out of the five monitoring stations (station 2 inside the paleochannel and station 5 outside) are shown in Figures 3, 4 and 5.

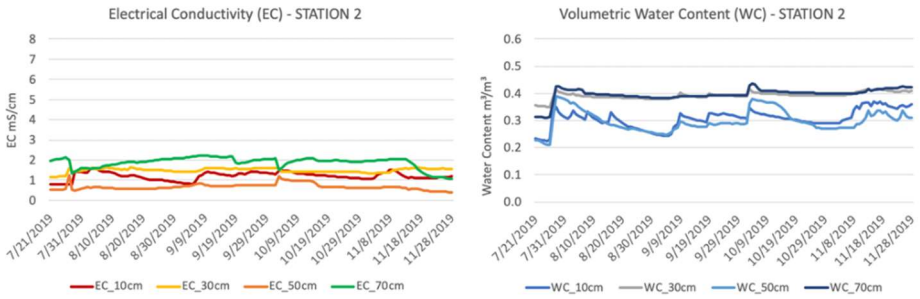

Fig. 87 -. Electrical conductivity and soil matric potential recorded at monitoring station 2 (inside the paleochannel)

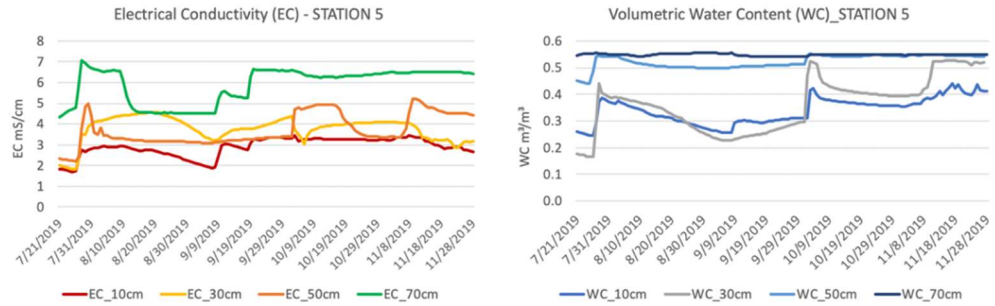

Fig. 88 -. Electrical conductivity and soil matric potential at monitoring station 5 (outside the paleochannel)

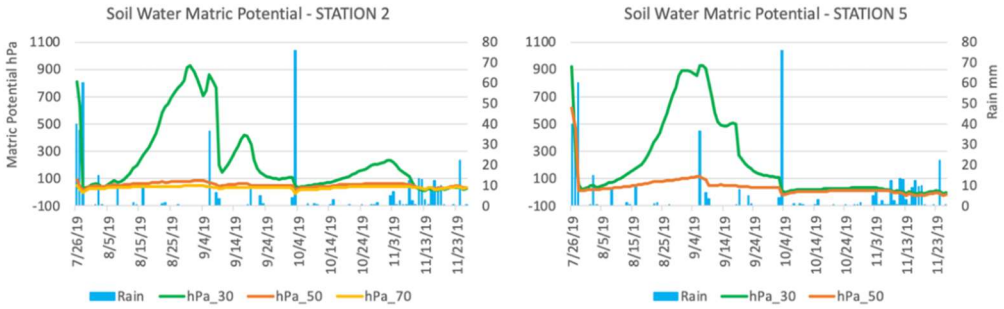

Fig. 89 -. Soil water matric potential recorded at station 2 (inside the paleochannel) and 5 (outside the paleochannels)

10. References

AGIP, 1994. Acque dolci sotterranee. Inventario dei dati raccolti dall'Agip durante la ricerca di idrocarburi in Italia dal 1971 al 1990. Roma, Italy, Agip S.p.A., p. 515.

Benvenuti G., Norinelli A., Zambrano R., 1973. Contributo alla conoscenza del sottosuolo dell'area circumlagunare veneta mediante sondaggi elettrici verticali. Boll. Geofisica Teorica e Applicata XV 57:23–38.

Bixio, A., Putti, M., Tosi, L., Carbognin, L., Gambolati, G., 1999. Finite element modeling of saltwater intrusion in the Venice aquifer system. In: Burganos, V.N., Karatzas, G.P., Payatakes, A.C., Brebbia, C.A., Gray, W.G., Pinder, G.F., Computational methods in surface and ground water transport. In: Computational mechanics publications ltd, Southampton, Hants, England, s04 2aaspringer verlag, vol. 12, London, p. 193-200, ISBN: 1-85312-653-5.

Carbognin, L., Tosi, L., 2003. Il progetto ISES per l'analisi dei processi di intrusione salina e subsidenza nei territori meridionali delle province di Padova e Venezia. Istituto per lo Studio della Dinamica delle Grandi Masse - CNR, Grafiche Erredici Padova (Italy), p. 95.

Carbognin, L., Gambolati, G., Putti, M., Rizzetto, F., Teatini, P., Tosi, L., 2006. Soil contamination and land subsidence raise concern in the Venice watershed, Italy. WIT Transactions on Ecology and the Environment 99:691-700.

Carbognin L, Teatini P, Tosi L (2010). The impact of relative sea level rise on the Northern Adriatic Sea coast, Italy. In: Carbognin L.; Teatini P.; Tosi L. (a cura di): Brebbia CA; Jovanovic N; Tiezzi E, MANAGEMENT OF NATURAL RESOURCES, SUSTAINABLE DEVELOPMENT AND ECOLOGICAL HAZARDS II. WIT TRANSACTIONS ON ECOLOGY AND THE ENVIRONMENT, vol. 127, p. 137-148 , ASHURST:WIT PRESS, ASHURST LODGE, SOUTHAMPTON SO40 7AA, ASHURST, ENGLAND, ISBN: 978-1-84564-204-4, ISSN: 1743-3541, Western Cape, SOUTH AFRICA , 15-17 December, 2009, doi: 137-148 DOI: 10.2495/RAV090121.

Da Lio, C., Tosi, L., Zambon, G., Vianello, A., Baldin, G., Lorenzetti, G., Manfè, G., Teatini, P., 2013. Long-term groundwater dynamics in the coastal confined aquifers of Venice (Italy). Estuar. Coast. Shelf S. 135:248-259.

Da Lio C, Carol E, Kruse E, Teatini P, Tosi L, 2015. Saltwater contamination in the managed low-lying farmland of the Venice coast, Italy: An assessment of vulnerability. SCIENCE OF THE TOTAL ENVIRONMENT, vol. 533, p. 356-369, doi: 10.1016/j.scitotenv.2015.07.013

de Franco, R., Biella, G., Tosi, L., Teatini, P., Lozej, A., Chiozzotto, B., Giada, M., Rizzetto, F., Claude, C., Mayer, A., Bassan, V., Gasparetto-Stori, G., 2009. Monitoring the saltwater intrusion by time lapse electrical resistivity tomography: The Chioggia test site (Venice Lagoon, Italy). J. of Appl. Geophys. 69(3-4):117-130.

Donnici, S., Serandrei-Barbero, R., Bini, C., Bonardi, M., Lezziero, A., 2011. The Caranto Paleosol and its role in the early urbanization of Venice. Geoarchaeology: An International Journal 26(4):514-543.

Gasparetto-Stori, G., Strozzi, T., Teatini, P., Tosi, L., Vianello, A., Wegmüller, U., 2012. DEM of the Veneto Plain by ERS2-ENVISAT Cross-Interferometry. Proc. of the 7th EUROGEO, 1:349-350.

Mayer A, Gattacceca J, Claude C, Radakovitch O, Giada M, Cucco A, Tosi L, Rizzetto F (2006). Radon activity in the southern Lagoon of Venice and the Adriatic Sea. In: (a cura di): Campostrini P., Scientific Research and Safeguarding of Venice 2005, CORILA Research, Research Program 2004-2006. vol. 4, p. 217-226, VENEZIA:CORILA, ISBN: 88-8940-507-4.

Rizzetto, F., Tosi, L., Carbognin, L., Bonardi, M., Teatini, P., 2003. Geomorphic setting and related hydrogeological implications of the coastal plain south of the Venice Lagoon, Italy. IAHS-AISH Publication 278:463-470.

Teatini, P., Gambolati, G., Tosi, L., 1995. A new 3-D non-linear model of the subsidence of Venice. In: Barends, F.B.J., et al. (Eds.), Land Subsidence. IAHS Publ. n. 234, Wallingford, UK, pp. 353e361.

Teatini P, Putti M, Rorai C, Mazzia A, Gambolati G, Tosi L, Carbognin L (2010). Modeling the saltwater intrusion in the lowlying catchment of the southern Venice Lagoon, Italy. In: (a cura di): Brebbia CA; Jovanovic N; Tiezzi E, MANAGEMENT OF NATURAL RESOURCES, SUSTAINABLE DEVELOPMENT AND ECOLOGICAL HAZARDS. WIT TRANSACTIONS ON ECOLOGY AND THE ENVIRONMENT, vol. 127, p. 351-362, ASHURST:WIT PRESS, ASHURST LODGE, SOUTHAMPTON SO40 7AA, ASHURST, ENGLAND, ISBN: 978-1-84564-204-4, ISSN: 1743-3541, Western Cape, SOUTH AFRICA , 15-17 December, 2009, doi: 10.2495/RAV090311

Teatini, P., Tosi, L., Viezzoli, A., Baradello, L., Zecchin, M., Silvestri, S., 2011. Understanding the hydrogeology of the Venice Lagoon subsurface with airborne electromagnetics. J. Hydrol. 411(3-4):342-354.

Tosi, L., Rizzetto, F., Bonardi, M., Donnici, S., Serandrei Barbero, R., Toffoletto, F., 2007. Note illustrative della Carta Geologica d'Italia alla scala 1: 50.000, Foglio 148-149 Chioggia-Malamocco, APAT, Dip. Difesa del Suolo, Servizio Geologico d'Italia, SystemCart, Roma, p. 164, 2 Maps.

Tosi, L., Rizzetto, F., Zecchin, M., Brancolini, G., Baradello, L., 2009. Morphostratigraphic framework of the Venice lagoon (Italy) by very shallow water VHRS surveys: evidence of radical changes triggered by human-induced river diversions. Geophys. Res. Lett. 36(9). doi: 10.1029/2008GL037136.

Tosi L, Di Sipio E, Carbognin L, Zuppi GM, Galgaro A, Teatini P, Bassan V, Vitturi A (2011). Intrusione salina. In: Monica Amatucci; Adriano Barbi; Valentina Bassan; Bruna Basso; Annelore Bezzi; Jacopo Boaga; Aldino Bondesan; Francesco Benincasa; Giuseppe Canali; Laura Carbognin; Enrico Conchetto; Andrea de Götzen; Elisa Destro; Eloisa Di Sipio; Chiara Fastelli; Alessandro Fontana; Giorgio Fontolan; Paola Furlanetto; Antonio Galgaro; Massimo Gattolin; Vittorio Iliceto; Chiara Levorato; Lucia Lovison Golob; Andrea Mazzuccato; Mirco Meneghel; Marco Monai; Paolo Mozzi; Simone Pillon; Sandra Primon; Roberta Racca; Francesca Ragazzi; Francesco Rech; Francesca Ronchese; Andrea Rosina; Roberto Rosselli; Tazio Strozzi; Pietro Teatini; Luigi Tosi; Gilmo Vianello; Andrea Vitturi; Paola Zamarchi; Pietro Zangheri; Giovanni Maria Zuppi. (a cura di): Andrea Vitturi, Atlante geologico della provincia di Venezia. Note Illustrative. p. 531-550, VENEZIA: Provincia di Venezia, ISBN: 978-88-907207-0-3

Tosi, L., Da Lio, C., Teatini, P., Menghini, A., and Viezzoli, A., 2018. Continental and marine surficial water – groundwater interactions: the case of the southern coastland of Venice (Italy), Proc. IAHS, 379, 387–392, https://doi.org/10.5194/piahs-379-387-2018.

Viezzoli, A., Tosi, L., Teatini, P., Silvestri, S., 2010. Surface water-groundwater exchange in transitional coastal environments by airborne electromagnetics: The Venice Lagoon example. Geophys. Res. Lett. 37(1). doi: 10.1029/2009GL041572.